Author Manuscript:
Published in final edited form as: *Surf. Interface Anal*. Volume 37, Issue 1, Pages 1 - 14 (2005).
https://doi.org/10.1002/sia.1997

Calculations of Electron Inelastic Mean Free Paths. VIII. Data for 15 Elemental Solids over the 50 eV to 2000 eV Range

S. Tanuma,[1] C. J. Powell,[2*] and D. R. Penn[2]

[1]Materials Analysis Station, National Institute for Materials Science, 1-2-1 Sengen, Tsukuba 305-0047, Japan

[2]National Institute for Standards and Technology, Gaithersburg, MD 20899, USA

We report calculations of electron inelastic mean free paths (IMFPs) for 50 eV to 2000 eV electrons in 14 elemental solids (Li, Be, diamond, graphite, Na, K, Sc, Ge, In, Sn, Cs, Gd, Tb, and Dy) and for one solid (Al) using better optical data than in our previous work. The new IMFPs have also been used to test our TPP-2M equation for estimating IMFPs in these materials. We found surprisingly large root-mean-square deviations (from 39.3 % to 71.8 %) between IMFPs calculated from TPP-2M and those calculated here from optical data for diamond, graphite, and cesium. An analysis showed that these deviations occurred for relatively small computed values of the parameter β in the TPP-2M equation ($\beta \sim 0.01$ for diamond and graphite) and for a relatively large value of β ($\beta \sim 0.25$ for Cs). While such extreme values of β are unlikely to be encountered for many other materials, the present results indicate an aditional limitation in the reliability of the TPP-2M equation. We also show that the parameter N_V in the TPP-2M equation should be computed for the rare-earth elements from the number of valence electrons and the six 5p electrons.

* Correspondence to: C. J. Powell, National Institute of Standards and Technology, Gaithersburg, MD 20899-8370, USA.
E-mail: Cedric.Powell@nist.gov.

Author Manuscript:
Published in final edited form as: *Surf. Interface Anal*. Volume 37, Issue 1, Pages 1 - 14 (2005).
https://doi.org/10.1002/sia.1997

INTRODUCTION

We have previously reported calculations of inelastic mean free paths (IMFPs) of 50 eV to 2000 eV electrons from experimental optical data for 27 elemental solids, 15 inorganic compounds, and 14 organic compounds, as well as analyses of these results.[1-7] The optical data were checked for internal consistency using two sum rules;[8] these checks indicated that the optical data for the group of elemental solids and the group of organic compounds were more reliable than those for the group of inorganic compounds. We therefore analyzed the IMFPs for the groups of elemental solids and organic compounds to derive an equation, designated TPP-2M, based on the Bethe equation[9] for inelastic scattering of electrons in matter.[5] We found that the four parameters in TPP-2M could be empirically related to several material parameters (atomic or molecular weight, density, number of valence electrons per atom or molecule, and the bandgap energy for nonconductors). The TPP-2M equation could then be used to estimate IMFPs for other materials over the 50 eV to 2000 eV energy range.

We report here IMFP calculations for 50 eV to 2000 eV electrons in an additional 14 elemental solids (Li, Be, diamond, graphite, Na, K, Sc, Ge, In, Sn, Cs, Gd, Tb, and Dy) and for one solid (Al) using better optical data than in our earlier work.[1,2] The new IMFPs are useful because they provide tests of TPP-2M for three additional classes of materials: alkali metals, allotropes of carbon, and rare-earth elements. The rare-earth elements have unusual electronic properties, and we discuss how TPP-2M should be evaluated for these elements.

IMFP CALCULATIONS

Our method for the IMFP calculation has been described previously.[1,2] We make use of the Penn[10] algorithm that is expected to give useful results for electron energies above 50 eV.[4] We also calculated IMFPs for energies between 10 eV and 40 eV, and display these results in the Figures below to show the IMFP trends *vs.* electron energy more completely; these results should be considered only as rough estimates. The IMFP values were calculated for most materials using Eq. (14) of Ref. 1 for electron energies between 10 eV and 200 eV and the simpler Eq. (16) of Ref. 1 was used for energies between 300 eV and 2000 eV; for graphite and Al, Eq. (14) was used for energies between 10 eV and 300 eV while Eq. (16) was used for energies of 400 eV and above. We note that the difference in IMFPs obtained using these two equations at 300 eV is very small (for example, less than 0.2 % for graphite). All energies are expressed with respect to the Fermi level.

Table 1 contains material-property data used in the IMFP calculations or in the later analysis of the IMFP results. We show there values of the atomic weight M, the bulk density ρ, the number of valence electrons per atom (N_v),[7] the free-electron plasmon energy ($E_p = 28.8(N_v\rho/M)^{1/2}$), the bandgap energy ($E_g$), and the Fermi energy (E_F). Data for glassy carbon are included in Table 1 and later Tables since IMFPs for this material[1,2] will also be analyzed.

The IMFPs were calculated using values of the energy loss function $\mathrm{Im}[-1/\varepsilon(\omega)]$, where $\varepsilon(\omega)$ is the complex dielectric constant for the material of interest as a function of photon energy $\hbar\omega$. Values of the energy loss function were calculated from the sources of optical data and energy-loss-function measurements listed in Table 2.[11-21] Since no direct

Author Manuscript:
Published in final edited form as: *Surf. Interface Anal.* Volume 37, Issue 1, Pages 1 - 14 (2005).
https://doi.org/10.1002/sia.1997

measurements were available for photon energies larger than about 40 eV, it was necessary to make use of atomic photoabsorption data for extrapolations to photon energies beyond the particular measurement range.[18] These extrapolations are not considered a serious source of error because $\varepsilon(\omega)$ for photon energies larger than about 40 eV is mainly determined by atomic properties except in the vicinity of core-electron excitation thresholds. The latter differences are unimportant in the IMFP calculation because an integration is made of the energy loss function over $\hbar\omega$.[1]

We evaluated the accuracy of our sets of $\mathrm{Im}[-1/\varepsilon(\omega)]$ data using two useful sum rules.[3,8] These sum rules are the oscillator-strength sum rule (or the f-sum rule) and a limiting form of the Kramers-Kronig integral (or KK-sum rule). The f-sum can be evaluated as the total effective number of electrons per atom Z_{eff} contributing to the inelastic scattering:[3,8]

$$Z_{eff} = (2/\pi\hbar^2\Omega_p^2)\int_0^{\Delta E_{\max}} \Delta E\, \mathrm{Im}[-1/\varepsilon(\Delta E)]d(\Delta E) \qquad (1)$$

where $\Delta E = \hbar\omega$, $\Omega_p = (4\pi n_a e^2/m)^{1/2}$, $n_a = N_a\rho/M$ is the density of atoms, and N_{a} is Avogadro's number. When the upper limit $\Delta E_{\max}$ in Eq. (1) is equal to infinity, Z_{eff} should be equal to Z, the total number of electrons per atom. The KK-sum can be expressed as:[3,8]

$$P_{eff} = (2/\pi)\int_0^{\Delta E_{\max}} \Delta E^{-1}\, \mathrm{Im}[-1/\varepsilon(\Delta E)]d(\Delta E) + n^{-2}(0) \qquad (2)$$

where $n(0)$ is the limiting value of the refractive index at low photon energies (below those where absorption maxima are observed). In the limit $\Delta E_{\max} \to \infty$, $P_{eff} \to 1$.

Table 3 lists the errors in the f-sum and KK-sum for the present group of materials from evaluations of Eqs. (1) and (2) with $\Delta E_{\max}$ = 30 keV. For $Z > 50$, we expect Z_{eff} to be less than Z since K-shell excitations cannot contribute to the integral of Eq. (1); for In (Z = 49) and Sn (Z = 50), the K-shell contributions are small (~ 0.1). Although there are two electrons in the K shell, the contributions of these electrons to the f-sum will be less than two.[9] Examination of Z_{eff} as a function of $\Delta E_{\max}$ for Na, Al, K, and Sc (elements that have K-shell binding energies appreciably less than 30 keV), for example, shows that the K-shell contributions to the f-sum integral range from 1.54 to 1.71 so that the average K-shell contribution for these elements is 1.65. For the elements In through Dy, Z_{eff} values from Eq. (1) were therefore compared with $(Z - 1.65)$ rather than with Z.

The average root-mean-square (RMS) error for the sets of $\mathrm{Im}[-1/\varepsilon(\Delta E)]$ data based on the f-sum rule is 4.0 % while that for the KK-sum is 8.4 %. The larger RMS error for the KK-sum is mainly due to the relatively large KK-sum errors for K and Sn. The KK-sum errors for these two materials must be associated with errors in the optical data for relatively low photon energies since the corresponding errors in the f-sum are much smaller.

The RMS error for the f-sum errors in Table 3 is less than a factor of two smaller than that for our original group of 27 elemental solids (9.9 %) while the RMS error for the KK-

Author Manuscript:
Published in final edited form as: *Surf. Interface Anal.* Volume 37, Issue 1, Pages 1 - 14 (2005).
https://doi.org/10.1002/sia.1997

sum is a little smaller than that for the original group (9.5 %).[1] We also note that the sum-rule errors for the new set of $\mathrm{Im}[-1/\varepsilon(\omega)]$ data for Al in Table 3 (1 % and 1.8 %) are appreciably smaller than the corresponding errors (12 % and 11 %) for the original set of Al data.[1]

As examples of our analysis and as material for later discussion, we show the energy-loss functions, $\mathrm{Im}[-1/\varepsilon(\Delta E)]$, of diamond, graphite, and glassy C[1,2] in Fig. 1 as a function of energy-loss, ΔE. These functions are also interesting because there is a common set of optical data for diamond and graphite from Ref. 18 for $\hbar\omega \geq 50$ eV (Table 2). The small differences in the magnitudes of $\mathrm{Im}[-1/\varepsilon(\Delta E)]$ for $\Delta E \geq 40$ eV are due to the different densities of diamond, graphite, and glassy C (Table 1). We also note here that values of $\mathrm{Im}[-1/\varepsilon(\Delta E)]$ for diamond and graphite were obtained from Refs. 19 and 20, respectively, rather than from Refs. 11 and 12 because the former data satisfied the sum rules [Eqs. (1) and (2)] much better than the latter data.

Figure 2 shows plots of M_{tot}^2 for the three forms of carbon as a function of $\Delta E_{\max}$, where

$$M_{tot}^2 = (2R/\pi\hbar^2\Omega_p^2)\int_0^{\Delta E_{\max}} \mathrm{Im}[-1/\varepsilon(\Delta E)]d(\Delta E) \qquad (3)$$

and R is the Rydberg energy (13.606 eV). The IMFP is inversely proportional to M_{tot}^2.[1] It is apparent from Fig. 2 that the larger contributions to M_{tot}^2 for carbon come from valence-electron excitations with ΔE values between 5 eV and 200 eV and much smaller contributions from K-shell excitations.

Figures 3 and 4 show plots of Z_{eff} and P_{eff}, respectively, for diamond, graphite, and glassy C as a function of $\Delta E_{\max}$. We see from Fig. 3 that Z_{eff} saturates for each material close to the expected value of $Z = 6$. It is clear from Fig. 4 that the main contributions to P_{eff} come from excitations with $\Delta E \leq 50$ eV.

IMFP RESULTS

Table 4 shows IMFPs calculated from the optical data for 50 eV to 2000 eV electrons in the 15 elemental solids. Plots of IMFP vs. electron energy for Li, Be, diamond, graphite, glassy C, Na, Al, Ge, In, Sn, and Cs are shown in Figs. 5-15 as examples of our results; IMFP results for glassy C[1,2] have been included here for comparison with those of diamond and graphite. Similar plots for K, Gd, Tb, and Dy have been published previously.[7] Information on uncertainties of the calculated IMFPs is given in our paper IV[4] and Ref. 22. The uncertainties of IMFPs for energies between 50 eV and 200 eV will be larger than those for higher energies.

As in our previous work,[2,3,5] we analyzed the IMFP dependence on energy for each material with a modified form of the Bethe equation[9] for inelastic electron scattering in matter:

$$\lambda = E/\{E_p^2[\beta\ln(\gamma E) - (C/E) + (D/E^2)]\} \qquad (4)$$

Author Manuscript:
Published in final edited form as: *Surf. Interface Anal.* Volume 37, Issue 1, Pages 1 - 14 (2005).
https://doi.org/10.1002/sia.1997

where λ is the IMFP (in Å), E is the electron energy (in eV), and β, γ, C, and D are parameters. The second and third terms in the denominator of Eq. (4) were added in order to describe the IMFP dependence on energy for energies less than 200 eV.[23,24] The solid lines in Figs. 5-15 show fits of Eq. (4) to the calculated IMFPs over the 50 eV to 2000 eV range. Values of β, γ, C, and D from the fits for each material are shown in Table 5.

To check our analysis, we have also calculated values of β valid for "high" electron energies. These values of β, denoted β_{opt}, represent the slopes of Fano plots (in which E/λ is plotted versus ln$E$) in the asymptotic Bethe region.[25] Values of β_{opt} can be obtained from the following relation:[3]

$$\beta_{opt} = M_{tot}^2 / 28.8 N_v \qquad (\text{eV}^{-1}\ \text{Å}^{-1}) \qquad (5)$$

We have evaluated M_{tot}^2 from Eq. (3) (with ΔE_{max} = 30 keV) and determined β_{opt} from Eq. (5); these values are shown in Table 5. We find that β_{opt} is typically less than β by amounts varying from 1 % (K) to 16 % (Ge) although β_{opt} exceeds β for graphite and Sc by 1 % and 6 %, respectively. It is expected[25] that the slopes of the Fano plots for energies between 50 eV and 2000 eV (given by β) should exceed the asymptotic slopes (given by β_{opt}).

We have previously analyzed calculated IMFPs for a group of 27 elemental solids[2] and a group of 14 organic compounds[5] and found that the four parameters in Eq. (4) could be related empirically to other material-property data:[5]

$$\beta = -0.10 + 0.944/(E_p^2 + E_g^2)^{0.5} + 0.069\rho^{0.1}, \qquad (6a)$$

$$\gamma = 0.191\rho^{-0.5}, \qquad (6b)$$

$$C = 1.97 - 0.91U, \qquad (6c)$$

$$D = 53.4 - 20.8U, \qquad (6d)$$

$$U = N_v\rho/M = E_p^2/829.4. \qquad (6e)$$

Equations (4) and (6) represent our TPP-2M formula for estimating IMFPs in materials.

The dashed lines in Figs. 5-15 indicate IMFPs calculated from TPP-2M and the data in Table 1. Table 6 shows values of the root-mean-square (RMS) deviations between IMFPs from TPP-2M and IMFPs calculated from optical data for the indicated materials. The unexpectedly large values of the RMS deviations for diamond (71.8 %), graphite (49.5 %), and Cs (39.3 %) will be discussed further below. If these three elements are disregarded, the average RMS deviation for the remaining elements is 11.8 %, only slightly larger than the average RMS deviation of 10.2 % for our original group of 27 elements.[5]

We have recently discussed the appropriate value for the parameter N_v (the number of valence electrons per atom) for certain elements where there has been ambiguity in the choice of this parameter.[7] Seah *et al.*[26] had earlier reported an analysis of Auger-electron intensities for 61 elemental solids and of photoelectron intensities for 58 elemental solids in which they

Author Manuscript:
Published in final edited form as: *Surf. Interface Anal.* Volume 37, Issue 1, Pages 1 - 14 (2005).
https://doi.org/10.1002/sia.1997

recommended that N_v be calculated from the number of electrons with binding energies less than or equal to 28 eV. The elements K, Gd, Tb, and Dy were among those for which there were differing recommendations for N_v that were discussed previously.[7] There were also different recommendations for the elements In, Sn, and Cs, and so we show IMFPs from TPP-2M in Figs. 13-15 for these elements that were obtained from values of N_v proposed by Seah *et al.* and ourselves.[7] These results will be discussed further below.

DISCUSSION

We will discuss the reliability of the TPP-2M equation for predicting IMFPs, the IMFP results for the low-density solids, and the choice of N_v in the TPP-2M equation for In, Sn, and Cs and for the rare-earth elements Gd, Tb, and Dy.

Reliability of the TPP-2M Equation

We first consider the IMFPs for the three allotropes of carbon in Figs. 7-9. At an energy of 2,000 eV, for example, the IMFPs calculated from optical data vary from 28.1 Å (diamond) to 31.6 Å (graphite) and 46.8 Å (glassy C) whereas the corresponding values from TPP-2M are almost identical (48.5 Å, 46.2 Å, and 46.3 Å). According to the Bethe theory for inelastic scattering of electrons in matter,[9] as further reviewed and discussed by Inokuti,[23] the total cross section, σ_{tot}, for inelastic scattering by an atom at a sufficiently high energy is proportional to M_{tot}^2. Since the IMFP is inversely proportional to the product of σ_{tot} and the density of atoms, we thus expect the IMFP for the three allotropes of carbon to be inversely proportional to ρM_{tot}^2 (where we have assumed, for simplicity, that there is no significant difference in the dependences of the energy-loss functions on momentum transfer for the three carbon allotropes).[6] Table 7 shows the asymptotic values of M_{tot}^2 for the three forms of carbon (for $\Delta E_{\max} = 30$ keV) and the values of $(\rho M_{tot}^2)^{-1}$. The values of $(\rho M_{tot}^2)^{-1}$ for diamond and graphite are 56 % and 66 % of those for glassy C; these percentages correspond closely to those found of IMFPs at 2,000 eV calculated from optical data (60 % and 67 %). Since the IMFPs from TPP-2M for diamond and graphite do not vary as expected from this simple analysis, we deduce that these values must have a much larger standard uncertainty than previously estimated for elemental solids.[5]

The large RMS deviations in Table 6 between IMFPs from the TPP-2M equation and IMFPs calculated from optical data for diamond, graphite, and Cs are not believed to be associated with inadequacies of the optical data for these solids (Table 2) because the errors in the f-sum and KK-sum rules are less than or comparable to those found for other elemental solids (Table 3, and Table 1 of paper I). To determine whether the large deviations in Table 6 might be associated in some way with extreme values of one or more of the parameters in Eqs. (4) and (6), we repeated key steps in the development of our TPP-2M equation.[5] This analysis was performed with IMFPs calculated from optical data for the previous groups of elemental solids,[1,2,7] inorganic compounds,[3,7] and organic compounds[5] with some exclusions and additions. We excluded IMFPs for materials with average errors in their f-sum and KK-sum evaluations exceeding 15 % (Nb, Al_2O_3, GaAs, InAs, InSb, LiF, and NaCl) and we

Author Manuscript:
Published in final edited form as: *Surf. Interface Anal.* Volume 37, Issue 1, Pages 1 - 14 (2005).
https://doi.org/10.1002/sia.1997

added IMFPs for some additional inorganic compounds (MgO, and a series of non-stoichiometric carbides of Ti, V, and Nb).[27]

Figure 16 shows a plot of "observed" values of β, β_{obs}, found from fits of Eq. (4) to the calculated IMFPs for each material versus $(E_p^2 + E_g^2)^{-0.5}$ (as shown in Fig. 10 of paper V). The long-dashed and short-dashed lines in Fig. 16 are plots of Eq. 6(a) with $\rho = 1$ g/cm^3 and $\rho = 10$ g/cm^3, respectively. There is a general linear trend of the plotted points but, as found previously, there are deviations that depend on density. The plotted point in Fig. 16 for Cs, however, lies appreciably above the lines. Since IMFPs computed from Eq. (4) are inversely proportional to β, we can conclude either that β_{obs} from the fit to IMFPs calculated from the Cs optical data is too large and thus the Cs IMFPs in Table 4 are smaller than they should be, or that β from Eq. 6(a) is too small and thus that IMFPs for Cs from TPP-2M (with $N_v = 1$, as shown in Table 1) are larger than they should be. We will comment further on the appropriate choice of N_v for Cs later.

Figure 17 shows a plot of $\beta_r = \beta_{obs} - 0.944(E_p^2 + E_g^2)^{-0.5}$ as a function of density (as suggested by Eq. 6(a) and as illustrated previously in Fig. 11 of paper V). The solid line is a plot of the variation expected from Eq. 6(a), namely $\beta_r = -0.10 + 0.069\,\rho^{0.1}$. It can be seen that most points scatter about the solid line although the point for Cs is again a significant outlier. A plot of $\beta_r + 0.1$ versus density on logarithmic scales (not shown) indicates that the points for Li and K in Fig. 17 deviate significantly from the linear dependence of the other points. It is not clear at present whether the deviations for Li and K in Fig. 17 are due to inadequacies of the IMFPs for these solids (e.g., as a result of unknown limitations of the optical data) or to inadequacies of Eq. 6(a). While it is possible that Eq. 6(a) could be modified to account for the low-density behavior exemplified by Li and K, we are reluctant to do this based on data for only two materials. In addition, it seems unlikely that TPP-2M would be used in practice for material densities appreciably less than those of the polymers examined in paper V.

Figure 18 shows plots, on two different scales, of β from Eq. 6(a) versus β_{obs}. As found previously for Fig. 12 of paper V, most points in Fig. 18 scatter about the dashed line $\beta = \beta_{obs}$. There are, however, deviations at both low and high values of β_{obs}. As expected from Figs. 16 and 17, the point for Cs in Fig. 18(b) (with the largest values of β and β_{obs} and the smallest value of E_p for the materials considered here) deviates appreciably from the dashed line. Despite the deviations of the points for Li and K from the lines in Figs. 16 and 17, the points for these solids lie reasonably close to the line in Fig. 18. As a result, the RMS deviations between IMFPs from TPP-2M and the IMFPs calculated from optical data for Li and K are reasonably small (13.8 % and 2.3 %, respectively, from Table 6). It is therefore unnecessary to modify TPP-2M further to account for the deviations of the points for these solids in Figs. 16 and 17.

We identify three points in Fig. 18(a) for low values of β_{obs}. While the absolute deviations of β for these points (diamond, graphite, and Pd) from the dashed line in Fig. 18(a) are less than the maximum deviation for other points, the relative deviation for each of these

three points is much larger. These large relative deviations lead to the substantial RMS deviations between IMFPs from TPP-2M and those from optical data (71.8 %, 49.5 %, and 20.1 % for diamond, graphite, and Pd,[5] respectively). The RMS deviation for Pd is appreciably less than those for diamond and graphite because the material parameters of Pd lead to lesser sensitivity to variations of β than for the other two materials.

Elastic-peak electron spectroscopy (EPES) has been identified as the preferred technique for measurements of IMFPs.[22] Two groups have made IMFP measurements by EPES for graphite,[28,29] and their results are plotted in Fig. 8; Lesiak *et al*.[29] have also reported similar measurements for glassy carbon, and these results are shown in Fig. 9. Most of the IMFPs reported by Tanuma *et al*.[29] for graphite agree better with IMFPs from TPP-2M rather than the IMFPs calculated from optical data; one value (at 250 eV) is much larger than expected from the energy dependence of nearby points, probably due to a diffraction effect. The graphite IMFPs of Lesiak *et al*.[28] show moderate scatter; some values in Fig. 8 are close to the TPP-2M curve while others are close to the solid line derived from the IMFPs computed from optical data. Overall, the general agreement of IMFPs from EPES with IMFPs from TPP-2M suggests that the TPP-2M equation is robust and that there must be some unexpected uncertainty in the graphite IMFPs obtained from optical data beyond that expected from the uncertainty in the corresponding optical data, as shown in Figs. 2 and 3 and as listed in Table 3, and in the model used for the IMFP calculation.[4,22] For glassy carbon, the measured IMFPs of Lesiak *et al*. in Fig. 9 are larger than both values from TPP-2M and from the optical data (which agree well with each other).

We need to point out that IMFPs derived from EPES measurements are based on a model in which it is assumed that elastic scattering of the backscattered electrons can be described by differential cross sections for elastic scattering by atoms in an amorphous or disordered solid.[22,30] The sample of interest is typically bombarded by rare-gas ions both to clean the surface and to amorphize the solid at least to the information depth for the detected EPES signal.[31] For crystalline samples such as diamond and graphite, an amorphized surface region might be sufficiently different in local atomic structure and bonding from the starting material to cause appreciable differences between the IMFPs derived from EPES experiments and those calculated from the optical data for the corresponding crystalline materials. In the experiments of Tanuma *et al*.,[29] however, the EPES measurements were performed without any ion sputtering. Further EPES experiments are needed to verify and extend the work of Lesiak *et al*. and Tanuma *et al.* (e.g., to perform the experiments at different scattering angles and/or with large analyzer acceptance angles for which diffraction effects might be shown to be minimal on samples that had had little or no ion bombardment). Additional tests should also be performed to characterize the surfaces before and after any ion bombardment; reflection electron energy-loss experiments could indicate, by comparison with energy-loss functions obtained from optical data (Fig. 1), whether a carbon sample was predominantly diamond, graphite, or glassy carbon. Additionally, Auger-electron spectroscopy can be utilized to distinguish the different forms of carbon.[32-34]

In principle, the large RMS deviations between IMFPs from TPP-2M and IMFPs calculated from optical data in Table 6 for diamond, graphite, and Cs could arise from

limitations of the TPP-2M equation, some unrecognized source of uncertainty in the optical data for these materials, and/or a deficiency of the algorithm used for the IMFP calculations. The optical data for these materials appear to be satisfactory, as revealed by our sum-rule checks (Figs. 2 and 3, and Table 3). In addition, there is a single prominent peak in the energy-loss function for each of these materials that can be identified as being due to bulk-plasmon excitation; these energy losses agrees within 13 % with the values of E_p in Table 1. The free-electron-gas expression of Lindhard and coworkers[35] for the dielectric function on which the Penn IMFP algorithm[10] is based would therefore appear to be valid.[4] By elimination, we believe that there is a limitation of the TPP-2M equation at extreme values of the parameter β. The large RMS deviations for diamond, graphite, and Cs in Table 6 occur for values of β that are smaller (diamond and graphite, where $\beta \sim 0.01$) than those for most other materials we have investigated to date and much larger (Cs, where $\beta \sim 0.25$) than those of other materials. We note that the first and third terms on the right-hand side of Eq. 6(a) are based on an empirical fit to deviations resulting from limitations of the second term in providing a value for β (as plotted in Fig. 17). As noted above, the fractional uncertainty in the derived β can be large when the values of β are small (as found for diamond, graphite, and Pd). A large uncertainty in the value of β for Cs (as suggested by Fig. 18(b)) could result simply from the fact that Eq. 6(a) is not valid for large values of β. Further IMFP calculations for materials with values of E_p and β_{obs} comparable to those of diamond, graphite and Cs would be required to determine whether a more complex expression than Eq. 6(a) would provide more reliable values of β for such materials.

Li, Be, Na, Al, K, and Cs

We were initially interested in IMFPs for Li, Be, Na, Al, K, and Cs for two main reasons. First, these solids have low densities, and we wished to check whether our TPP-2M equation, developed mainly from computed IMFPs for high-density metals and low-density polymers,[5] would be valid for relatively light metals. Second, four of the solids are alkali metals, a class of solids that we had not previously investigated. Although there was no reason to expect that IMFPs for alkali metals would be qualitatively different from those for other solids (other than being generally larger, as illustrated by the results in Table 4, because of their lower densities), we wished to compute IMFPs for as many different types of solids as possible.

The RMS deviations in Table 6 between IMFPs from the TPP-2M equation [Eqs. (4) and (6)] for Li, Be, Na, Al, and K vary between 2.3 % (for K) and 25.3 % (for Be); the RMS deviation for Cs was discussed in the previous section. The RMS deviations for Li, Be, Al, and K are comparable to those found for our original groups of 27 elemental solids and 14 organic compounds for which the average RMS deviations were 10.2 % and 8.5 %, respectively.[5] We also note that the new RMS deviation for Al (12.7 %) is much smaller than that we found previously (22.7 %)[5] when we computed IMFPs from what we now know to be an inferior set of optical data.[1,2]

Choice of N_v in the TPP-2M Equation

Author Manuscript:
Published in final edited form as: *Surf. Interface Anal*. Volume 37, Issue 1, Pages 1 - 14 (2005).
https://doi.org/10.1002/sia.1997

We have recently discussed the appropriate choice of the parameter N_v in the TPP-2M equation and have pointed out that there can be ambiguity in choosing a value of this parameter for some elements.[7] This ambiguity arises for elements with shallow core levels (generally with binding energies less than about 30 eV) that may contribute significant intensity to the energy-loss function. As a result, the IMFP estimated from TPP-2M with N_v computed only from the number of valence electrons may be an overestimate of the IMFP.[7]

Figures 13-15 show IMFPs computed from TPP-2M for In, Sn, and Cs where N_v has been calculated from the number of valence electrons for each element and from the values recommended by Seah *et al*.[26] (M. P. Seah and I. S. Gilmore, personal communication). From an analysis of measured Auger-electron and photoelectron intensities for some 60 elemental solids, Seah *et al*. recommended that N_v be computed from the number of electrons with binding energies less than or equal to 28 eV. Figure 14 for Sn shows that IMFPs obtained from TPP-2M with $N_v = 4$ agree much better with the IMFPs from optical data than values obtained with $N_v = 14$. For In and Cs, however, the IMFPs calculated from optical data are roughly midway between those obtained from TPP-2M with the alternative values of N_v. The RMS deviations between IMFPs from TPP-2M with the alternative values of N_v and IMFPs from the optical data are 15.1 % and 39.5 % for In and Cs, respectively; these RMS deviations are comparable to those listed in Table 6 (19.5 % and 39.3 %, respectively) for the N_v values listed in Table 1.

Before commenting further on the N_v results for In, Sn, and Cs, we turn to similar results for Gd, Tb, and Dy in Figs. 4-6 of paper VII.[7] We recommended there that, for the rare-earth elements, N_v should be computed from the sum of the number of valence electrons for the solid state, either two or three as discussed by Netzer and Matthew,[36] and the six 5p electrons that contribute strongly to the energy-loss function. Although the 5p electrons for the lanthanides have binding energies between 18 eV and 27 eV,[37] they have been included in the calculation of N_v because of the strong 5p-6d excitations that occur close to the threshold energy for excitation (i.e., the binding energy).[38] In contrast, the number of 4f electrons has not been included in the N_v calculation, even though they have binding energies of less than 9 eV.[39] The 4f orbitals are highly localized, and they contribute weakly to the energy-loss function because of the substantial "delayed onsets" in plots of photoabsorption cross section versus photon energy.

We now consider the plot in Fig. 19(a) of the energy-loss function for Gd as representative of those for other lanthanide elements.[38] Here and in following plots, we show the energy-loss function for energy losses up to 200 eV to show the relative contributions of valence-electron and shallow-core-electron excitations to the IMFP. The strongest feature in Fig. 19(a), an energy-loss at about 13 eV, is due to bulk-plasmon excitation.[38] This energy-loss is close to the calculated free-electron bulk-plasmon energy (based on three valence electrons/atom) of 11.4 eV. Although the 5p electrons in Gd are core levels (with a $5p_{3/2}$ binding energy of 21.4 eV),[37] they contribute strongly to the energy-loss function due to a strong 5p → 5d resonance excitation.[38] In contrast, excitations of 4f electrons (with a binding energy of about 8 eV)[37] are relatively weak with no obvious structure. Excitations of 4d electrons begin at the expected $4d_{3/2}$ threshold (about 141 eV).[37]

Author Manuscript:
Published in final edited form as: *Surf. Interface Anal.* Volume 37, Issue 1, Pages 1 - 14 (2005).
https://doi.org/10.1002/sia.1997

Figures 19(b) and 19(c) show plots of Z_{eff} and M_{tot}^2, respectively, for Gd as a function of $\Delta E_{\max}$ from evaluations of Eqs. (1) and (3). It is clear from Fig. 19(b) that $Z_{eff} \approx 9$ (the value of N_v given in Table 1 for Gd, Tb, and Dy) when $\Delta E_{\max}$ reaches 50 eV; the seven 4f electrons[36] in Gd contribute to the monotonic increase of Z_{eff} in Fig. 19(b) with increasing $\Delta E_{\max}$ until the beginning of the 4d excitations at $\Delta E_{\max} = 141$ eV. It is clear from Fig. 19(c), however, that the valence and 5p excitations in Gd contribute strongly to the value of M_{tot}^2 while other excitations are responsible for the gradual increase of M_{tot}^2 for $\Delta E_{\max} > 50$ eV. The asymptotic value of M_{tot}^2 is 4.71 while the value of M_{tot}^2 for $\Delta E_{\max} = 50$ eV is about 3.13. Unlike the situation for C in Fig. 4 where core-electron excitations contribute minimally to the value of M_{tot}^2, such excitations with $\Delta E > 50$ eV contribute about 34 % of the value of M_{tot}^2 and thus to the IMFP.[1,2] Nevertheless, it is apparent from Fig. 4 of paper VII that variation of N_v in TPP-2M for Gd from 9 to 16 decreases the derived IMFP by less than 12 %. The choice of $N_v = 9$ is thus justified by the strong contributions of the three valence and six 5p electrons to the loss spectrum (for energy losses less than 50 eV) and the dominant contribution of these excitations to M_{tot}^2.

We now discuss further the choice of N_v in TPP-2M for In, Sn, and Cs. Figures 20(a) and 21(a) shows the energy-loss functions of Cs and Sn, respectively. The energy-loss function for Cs is similar to that of Gd in Fig. 19(a), with a strong bulk-plasmon excitation of the valence electrons at an energy loss of 3.1 eV (close to the free-electron value of 3.43 eV) and excitations of 5p and 4d electrons (with binding energies of about 12.2 and 75 eV, respectively).[37] Plots of Z_{eff} and M_{tot}^2 for Cs in Figs. 20(b) and 20(c) show clear plateaus in the vicinity of $\Delta E_{\max} = 50$ eV. The value of Z_{eff} increases from 5.9 at $\Delta E_{\max} = 50$ eV to 6.2 at $\Delta E_{\max} = 74$ eV, while M_{tot}^2 is about 6.6 at $\Delta E_{\max} = 50$ eV compared to the asymptotic value of 8.52 at $\Delta E_{\max} = 30$ keV. As for Gd and the other rare-earth elements, it now appears that we should include the six 5p electrons in the count of N_v for Cs; that is, N_v for Cs should be 7 instead of 1. The dot-dashed line in Fig. 15 shows IMFPs computed from TPP-2M with this value of N_v. The IMFP values are only slightly larger than those for $N_v = 9$, and the RMS deviation between IMFPs obtained with $N_v = 7$ and the IMFPs calculated from optical data is 34.9 %, only a slight reduction from the value of 39.3 % found with $N_v = 1$. We conclude that, while $N_v = 7$ for Cs appears to be a better choice than $N_v = 1$, there is still substantial disagreement with IMFPs obtained from optical data. The value of β from TPP-2M is now 0.0777 (instead of 0.249 with $N_v = 1$), and the point for Cs in Fig. 18(b) would lie much further from the dashed line than the plotted Cs point. Further tests of TPP-2M are therefore required to assess its validity for relatively large values of β and β_{obs}.

We now consider the choice of N_v for In and Sn which have similar energy-loss functions. The energy-loss function for Sn in Fig. 21(a) shows a strong volume-plasmon with an energy loss of 14 eV, close to the free-electron value of 14.3 eV with $N_v = 4$. Other features in Fig. 21(a) can be identified as being due to excitations of 4d and 4p electrons

Author Manuscript:
Published in final edited form as: *Surf. Interface Anal.* Volume 37, Issue 1, Pages 1 - 14 (2005).
https://doi.org/10.1002/sia.1997

(with binding energies of about 24 and 85 eV, respectively).[37] The plot of Z_{eff} for Sn in Fig. 21(b) shows a step at about $\Delta E_{max} = 20$ eV, where Z_{eff} = 1.82, and a monotonic increase for larger values of ΔE_{max} with a plateau in the vicinity of $\Delta E_{max} = 150$ eV where Z_{eff} = 18.0; this plot is qualitatively different from the corresponding plot for Cs in Fig. 20(b). The plot of M_{tot}^2 for Sn in Fig. 21(c) shows a step at about $\Delta E_{max} = 20$ eV (where $M_{tot}^2 = 1.80$) and an increase to a plateau at about 150 eV (where $M_{tot}^2 = 5.09$). The asymptotic value of M_{tot}^2 is 5.58 (for $\Delta E_{max} = 30$ keV). These results suggest that the ten 4d electrons should be included in the count of N_v although Fig. 14 indicates that this would lead to larger deviations of the TPP-2M IMFPs from the values computed from optical data. While the arguments based on Fig. 21 indicate that N_v =14 would be a better choice than N_v = 4, the opposite conclusion is reached from Fig. 14. For In, plots of Z_{eff} and M_{tot}^2 versus ΔE_{max} are similar to those for Sn in Figs. 21(b) and (c). The IMFPs computed from optical data for In in Fig. 13, however, are roughly midway between those obtained from TPP-2M with N_v = 3 and N_v = 13. Experimental IMFP measurements are therefore required to test whether the IMFPs for In and Sn derived from optical data are correct and/or whether the N_v values for these solids in Table 1 should be revised to include ten 4d electrons.

SUMMARY

We report results of IMFP calculations for 50 eV to 2000 eV electrons in 14 elemental solids (Li, Be, diamond, graphite, Na, K, Sc, Ge, In, Sn, Cs, Gd, Tb, and Dy) and for one solid (Al) using better optical data than in our earlier work.[1,2] The new IMFPs have also been used to test our TPP-2M equation[5] for estimating IMFPs in additional classes of materials (alkali metals, allotropes of carbon, and rare-earth elements).

We found unexpectedly large RMS deviations between IMFPs calculated from TPP-2M and IMFPs derived from optical data for three solids: diamond (71.8 %), graphite (49.5 %), and Cs (39.3 %). We analyzed possible origins of these large RMS deviations, and concluded that they occurred for extreme values of the parameter β in TPP-2M, as calculated from Eq. (6a). When the calculated value of β is small (~ 0.01), as it is for diamond and graphite, the relative uncertainty of β can be large. When the calculated value of β is large (~ 0.25), as it is for Cs, TPP-2M does not provide reliable IMFPs. Fortunately, for current applications, there seem to be few materials for which such extreme values of β will be encountered. Unfortunately, the lack of materials with these extreme values of β makes it difficult for us to derive empirical modifications of Eq. (6a) for such situations.

We recently discussed the appropriate choice of the parameter N_v in TPP-2M.[7] For most elements, we recommended that N_v be calculated in most cases from the number of valence electrons per atom in a given solid. For the rare-earth elements, however, we recommended that N_v be computed from the sum of the number of valence electrons in the solid state (either two or three) and the six 5p electrons that have binding energies between 18 eV and 27 eV. We provide a rationale here for this choice using Gd as an example. Due to a resonance excitation,[38] the Gd 5p electrons contribute strongly to the energy-loss function

Author Manuscript:
Published in final edited form as: *Surf. Interface Anal*. Volume 37, Issue 1, Pages 1 - 14 (2005).
https://doi.org/10.1002/sia.1997

and to the IMFP. In contrast, the 4f electrons contribute weakly to the energy-loss function and IMFP. The same rationale indicates that the six 5p electrons of Cs should be included in the count for N_v; this choice, however, does not significantly reduce the RMS deviation between IMFPs from TPP-2M and those from optical data. We also consider inclusion of the ten 4d electrons in the count of N_v for In and Sn since these electrons also contribute strongly to the energy-loss function. Experimental IMFP measurements will be needed to test whether the N_v values for these elements should be revised to include ten 4d electrons.

Author Manuscript:
Published in final edited form as: *Surf. Interface Anal*. Volume 37, Issue 1, Pages 1 - 14 (2005).
https://doi.org/10.1002/sia.1997

REFERENCES

1. Tanuma S, Powell CJ, Penn DR. *Surf. Interface Anal.* 1988; **11**: 577, Paper I in this series.
2. Tanuma S, Powell CJ, Penn DR. *Surf. Interface Anal.* 1991; **17**: 911, Paper II in this series.
3. Tanuma S, Powell CJ, Penn DR. *Surf. Interface Anal.* 1991; **17**: 929, Paper III in this series.
4. Tanuma S, Powell CJ, Penn DR. *Surf. Interface Anal.* 1993; **20**: 77, Paper IV in this series.
5. Tanuma S, Powell CJ, Penn DR. *Surf. Interface Anal.* 1994; **21**: 165, Paper V in this series.
6. Tanuma S, Powell CJ, Penn DR. *Surf. Interface Anal.* 1997; **25**: 25, Paper VI in this series.
7. Tanuma S, Powell CJ, Penn DR. *Surf. Interface Anal.* 2003; **35**: 268, Paper VII in this series.
8. Tanuma S, Powell CJ, Penn DR. *J. Electron Spectrosc. Relat. Phenom.*. 1993; **62**: 95.
9. Bethe H. *Ann. der Physik* 1930; **5**: 325.
10. Penn DR. *Phys. Rev. B* 1987; **35**: 482.
11. *Handbook of Optical Constants of Solids*, ed. by E. D. Palik, Academic Press, New York (1985).
12. *Handbook of Optical Constants of Solids II*, ed. by E. D. Palik, Academic Press, New York (1991).
13. *Handbook of Optical Constants of Solids III*, ed. by E. D. Palik, Academic Press, New York (1998).
14. Brousseau-Lahaye B, Colliex C, Frandon J, Gasgnier M, Trebbia P. *Phys. Stat. Sol. (b)* 1975; **69**: 257.
15. Marton L, Toots J. *Phys. Rev.* 1967; **160**: 602.
16. Daniels, J. *Opt. Commun.* 1971; 3: 13.
17. Colliex C, Gasgnier M, Trebbia P. *J. de Phys.* 1976; **37**: 397.
18. Henke BL, Davis JC, Gullikson EM, Perera RCC. Lawrence Berkeley Laboratory Report 26259 (1988); Henke BL, Gullikson EM, Davis JC. *At. Data Nucl. Data Tables* 1993; **54**: 181.
19. Daniels J, von Festernberg C, Raether H, Zeppenfeld K. *Springer Tracts in Modern Physics* 1970; **54**: 77.
20. Venghaus H. *Phys. Stat. Sol. (b)* 1975; **71**: 609.
21. Hagemann H-J, Gudat W, Kunz C. Deutsches Elektronen-Synchrotron Report SR-74/7 (1974); Hagemann H-J, Gudat W, Kunz C. *J. Opt. Soc. Am.* 1975; **65**: 742.
22. Powell CJ, Jablonski, A. *J. Phys. Chem. Ref. Data* 1999; **28**: 19.
23. Inokuti M. *Rev. Mod. Phys.* 1971; **43**: 297.
24. Ashley JC. *J. Electron Spectrosc. Relat. Phenom.* 1982; **28**: 177.
25. Powell CJ. *Surf. Interface Anal.* 1987; **10**: 349; *Ultramicroscopy* 1989; **28**: 24.
26. Seah, MP, Gilmore IS, Spencer SJ. *Surf. Interface Anal.* 2001; **31**: 778.
27. Tanuma S, Powell CJ, Penn DR (to be published).
28. Lesiak B, Jablsonki A, Prussak Z, Mrozek P. *Surf. Science* 1989; **223**: 213.

Author Manuscript:
Published in final edited form as: *Surf. Interface Anal*. Volume 37, Issue 1, Pages 1 - 14 (2005).
https://doi.org/10.1002/sia.1997

29. Tanuma S, Goto K, Ichimura S (to be published).
30. Jablonski A, Salvat F, Powell CJ. *J. Phys. Chem. Ref. Data* 2004; **33**: 409.
31. Jablonski A, Powell CJ. *Surf. Science* 2004; **551**: 106.
32. Haas TW, Grant JT, Dooley, GJ. *J. Appl. Phys.* 1972; **43**: 1853.
33. Steffen HJ, Roux CD, Marton D, Rabalais JW. *Phys. Rev. B* 1991; **44**: 3981.
34. Ramaker DE, in *Surface Analysis by Auger and X-Ray Photoelectron Spectroscopy*, D. Briggs and J. T. Grants, eds. IM Publications: Chichester, 2003, p. 465.
35. Lindhard J, Scharff. *K. Dan. Vidensk. Selsk. Mat.-Fys. Medd.* 1953; **27**: No. 15; Lindhard J, Scharff M, Schiott HE. *K. Dan. Vidensk. Selsk. Mat.-Fys. Medd.* 1963; **33**: No. 14.
36. Netzer F, Matthew JAD. *Rep. Prog. Phys*. 1986; **49**: 621.
37. Wagner CD, Naumkin AV, Kraut-Vass A, Allison JW, Powell CJ, Rumble JR. *NIST X-ray Photoelectron Spectroscopy Database*, SRD 20, Version 3.4; http://srdata.nist.gov/xps.
38. Netzer FP, Matthew JAD, in *Handbook on the Physics and Chemistry of Rare Earths*, K. A. Gschneidner, L. Eyring, and S. Hufner, eds. North-Holland: Amsterdam, 1987, Vol. 10, p.547.
39. Cardona M, Ley L (eds). *Photoemission in Solids I*. Springer-Verlag: Berlin, 1978.

Author Manuscript:
Published in final edited form as: *Surf. Interface Anal.* Volume 37, Issue 1, Pages 1 - 14 (2005).
https://doi.org/10.1002/sia.1997

Table 1. Values of the material parameters used in the IMFP calculations and the analysis of the IMFP results for the indicated materials.

Material	M	ρ (g cm^{-3})	N_v	E_p (eV)	E_g (eV)	E_F (eV)
Li	6.941	0.534	1	7.99	0	4.74
Be	9.0122	1.848	2	18.44	0	14.3
Diamond	12.011	3.515	4	31.16	5.5	20.4
Graphite	12.011	2.25	4	24.93	0	20.4
Glassy C	12.011	1.8	4	22.30	0	20.4
Na	22.9898	0.971	1	5.92	0	3.24
Al	26.9815	2.699	3	15.78	0	11.2
K	39.0983	0.862	1	4.28	0	2.12
Sc	44.9559	2.989	3	12.86	0	5.8
Ge	72.59	5.32	4	15.59	0.67	12.6
In	114.818	7.31	3	12.59	0	4.82
Sn	118.71	7.31	4	14.29	0	5.51
Cs	132.905	1.88	1	3.43	0	1.73
Gd	157.25	8.23	9	19.77	0	3.5
Tb	158.9253	8.25	9	19.69	0	4.0
Dy	162.5	8.78	9	20.08	0	3.5

—

Author Manuscript:
Published in final edited form as: *Surf. Interface Anal*. Volume 37, Issue 1, Pages 1 - 14 (2005).
https://doi.org/10.1002/sia.1997

Table 2. Sources of optical data and energy-loss-function measurements used in the IMFP calculations.

Material	Photon energy range (eV)	Source of data
Li	0.14 – 10.6	Ref. 12
	12 – 28	Interpolation of energy-loss-function data with $a\Delta E^n$ equation
	30 – 30,000	Ref. 18
Be	0.02 – 300	Ref. 12
	300 – 30,000	Ref. 18
Diamond	5.5 – 45	Ref. 19
	45 – 30,000	Ref. 18
Graphite	0.02 – 40	Ref. 20
	50 – 30,000	Ref. 18
Glassy C	0.1 – 30,000	Ref. 21
Na	0.55 – 4	Ref. 12
	4 – 9	Interpolation of extinction-coefficient data with a linear equation
	9 – 34	Ref. 12 (extinction-coefficient data)
	4 – 34	Interpolation of refractive-index data using cubic-spline function
	35 – 30,000	Ref. 18

Table 2 (continued)

Al	0.04 – 10,000	Ref. 11

Author Manuscript:
Published in final edited form as: *Surf. Interface Anal*. Volume 37, Issue 1, Pages 1 - 14 (2005).
https://doi.org/10.1002/sia.1997

	10,044 – 30,000	Ref. 18
K	0.55 – 10.33	Ref. 12
	11 – 32	Interpolation of refractive-index data with a linear equation
	11 – 32	Ref. 12 (extinction-coefficient data)
	35 – 30,000	Ref. 18
Sc	1.4 – 48.2	Ref. 14
	49 – 30,000	Ref. 18
Ge	0.7 – 7	Ref. 11
	7.66 – 25.2	Ref. 15
	26 – 30	Interpolation with a quintic equation
	30.7 – 30,000	Ref. 18
In	0.12 – 16.75	Ref. 13
	17 – 28.5	Interpolation of refractive-index data with a linear equation
	17 – 28.5	Ref. 13 (extinction-coefficient data)
	30 – 30,000	Ref. 18
Sn	0.1 – 21	Ref. 13
	23 – 50	Interpolation of refractive-index data with a quartic equation
	23 – 50	Ref. 13 (extinction-coefficient data)

Author Manuscript:
Published in final edited form as: *Surf. Interface Anal*. Volume 37, Issue 1, Pages 1 - 14 (2005).
https://doi.org/10.1002/sia.1997

Table 2 (continued)

	50.9 – 30,000	Ref. 18
Cs	0.51 – 30	Ref. 13
	31.5 – 30,000	Ref. 18
Gd	0.9 – 39.7	Ref. 16
	50 – 30,000	Ref. 18
Tb	0.5 – 46.6	Ref. 17
	50.9 – 30,000	Ref. 18
Dy	1.3 – 49.6	Ref. 16
	52.3 – 30,000	Ref. 18

Author Manuscript:
Published in final edited form as: *Surf. Interface Anal*. Volume 37, Issue 1, Pages 1 - 14 (2005).
https://doi.org/10.1002/sia.1997

Table 3. Errors in the f-sum [Eq. (1)] and the KK-sum [Eq. (2)] rules for the indicated materials with ΔE_{max} = 30 keV. For In, Sn, Cs, Gd, Tb, and Dy, the f-sum error was evaluated by comparing Z_{eff} from Eq. (1) with Z – 1.65 instead of Z as described in the text.

Material	Error in f-sum rule (%)	Error in KK-sum rule (%)
Li	2.1	1.8
Be	2.4	6.6
Diamond	-0.5	-0.2
Graphite	4.8	7.7
Glassy C	-3.9	-0.2
Na	1.2	3.5
Al	1.0	1.8
K	-6.8	-17.0
Sc	9.0	-7.5
Ge	2.0	4.2
In	-0.2	-8.3
Sn	0.6	-23.1
Cs	-7.5	0.4
Gd	-0.1	2.6
Tb	2.4	6.6
Dy	3.2	-1.2

Author Manuscript:
Published in final edited form as: *Surf. Interface Anal.* Volume 37, Issue 1, Pages 1 - 14 (2005). https://doi.org/10.1002/sia.1997

Table 4. Inelastic mean free paths as a function of energy for 15 elemental solids.

Electron energy (eV)	Inelastic mean free path (Å)														
	Li	Be	Diamond	Graphite	Na	Al	K	Sc	Ge	In	Sn	Cs	Gd	Tb	Dy
50	4.6	3.5	6.9	4.8	5.0	3.5	7.1	4.6	4.0	4.7	5.8	6.3	4.1	4.1	4.5
100	7.0	4.3	4.7	4.4	7.6	4.6	10.0	4.9	5.0	5.4	6.4	9.3	4.6	4.2	4.6
150	9.2	5.2	5.1	5.2	9.8	5.7	12.8	5.6	6.1	6.3	7.3	12.1	5.5	4.9	5.2
200	11.3	6.2	5.7	6.0	11.8	6.8	15.6	6.5	7.2	7.1	8.2	14.8	6.5	5.7	6.0
300	15.3	8.2	7.1	7.6	15.8	8.9	21.2	8.4	9.3	8.8	10.0	20.0	8.4	7.3	7.7
400	19.0	10.0	8.5	9.3	19.5	10.9	26.4	10.2	11.1	10.6	11.9	24.7	10.1	8.8	9.2
500	22.7	11.7	9.9	10.8	23.1	12.7	31.4	11.9	12.9	12.3	13.8	29.3	11.8	10.2	10.6
600	26.2	13.4	11.3	12.4	26.6	14.5	36.3	13.7	14.6	14.0	15.6	33.8	13.4	11.6	12.1
700	29.7	15.1	12.6	13.9	30.1	16.3	41.1	15.4	16.3	15.7	17.5	38.1	15.0	13.0	13.5
800	33.1	16.7	13.9	15.4	33.4	18.0	45.8	17.0	18.0	17.4	19.3	42.4	16.5	14.3	14.8
900	36.4	18.3	15.1	16.8	36.8	19.7	50.3	18.6	19.6	19.0	21.0	46.7	18.0	15.6	16.2
1000	39.7	19.9	16.4	18.2	40.0	21.3	54.8	20.2	21.2	20.6	22.8	50.8	19.5	16.9	17.5
1100	43.0	21.5	17.6	19.6	43.3	23.0	59.2	21.8	22.8	22.1	24.5	54.9	21.0	18.2	18.8
1200	46.2	23.0	18.8	21.0	46.5	24.6	63.6	23.3	24.4	23.7	26.2	59.0	22.5	19.5	20.1
1300	49.4	24.5	20.0	22.3	49.6	26.2	67.9	24.9	26.0	25.2	27.8	63.0	23.9	20.7	21.4
1400	52.6	26.1	21.2	23.7	52.7	27.8	72.2	26.4	27.5	26.7	29.5	67.0	25.4	22.0	22.7

Author Manuscript:
Published in final edited form as: *Surf. Interface Anal*. Volume 37, Issue 1, Pages 1 - 14 (2005). https://doi.org/10.1002/sia.1997

1500	55.7	27.6	22.4	25.0	55.8	29.4	76.4	27.9	29.0	28.1	31.1	71.0	26.8	23.2	23.9
1600	58.8	29.0	23.5	26.4	58.9	31.0	80.6	29.3	30.5	29.6	32.7	74.9	28.2	24.4	25.1
1700	61.9	30.5	24.7	27.7	62.0	32.6	84.8	30.8	32.0	31.0	34.3	78.7	29.6	25.6	26.4
1800	65.0	32.0	25.8	29.0	65.0	34.1	88.9	32.3	33.5	32.5	35.8	82.6	31.0	26.8	27.6
1900	68.0	33.4	27.0	30.3	68.0	35.6	93.0	33.7	35.0	33.9	37.4	86.4	32.3	28.0	28.8
2000	71.0	34.9	28.1	31.6	71.0	37.2	97.1	35.1	36.5	35.3	38.9	90.2	33.7	29.2	30.0

Author Manuscript:
Published in final edited form as: *Surf. Interface Anal*. Volume 37, Issue 1, Pages 1 - 14 (2005).
https://doi.org/10.1002/sia.1997

Table 5. Values of the parameters β, γ, C, and D found in the fits of Eq. (4) to the IMFP data for each material together with values of β_{opt} calculated from Eq. (5).

Material	β_{opt} (eV^{-1} $Å^{-1}$)	β (eV^{-1} $Å^{-1}$)	γ (eV^{-1})	C ($Å^{-1}$)	D (eV $Å^{-1}$)
Li	0.0646	0.0670	0.370	2.43	58.8
Be	0.0279	0.0305	0.130	1.07	14.8
Diamond	0.0123	0.0138	0.104	1.30	26.4
Graphite	0.0190	0.0188	0.117	1.19	18.2
Glassy C	0.0147	0.0159	0.117	0.91	18.4
Na	0.1236	0.1306	0.243	5.95	202.6
Al	0.0367	0.0422	0.086	0.46	13.9
K	0.1726	0.1746	0.316	5.31	9.1
Sc	0.0604	0.0569	0.217	6.55	152.1
Ge	0.0409	0.0484	0.054	0.17	17.8
In	0.0672	0.0725	0.073	4.12	140.1
Sn	0.0485	0.0544	0.054	2.43	93.8
Cs	0.2960	0.3177	0.196	3.33	43.0
Gd	0.0279	0.0303	0.078	0.85	16.9
Tb	0.0327	0.0345	0.087	1.85	43.0
Dy	0.0311	0.0330	0.077	1.79	47.2

Author Manuscript:
Published in final edited form as: *Surf. Interface Anal*. Volume 37, Issue 1, Pages 1 - 14 (2005).
https://doi.org/10.1002/sia.1997

Table 6. Root-mean-square (RMS) deviations between IMFPs from TPP-2M [Eqs. (4) and (6) and the values of N_v in Table 1] and IMFPs calculated from optical data for the indicated materials and energies between 50 eV and 2,000 eV.

Material	RMS deviation (%)
Li	13.8
Be	25.3
Diamond	71.8
Graphite	49.5
Glassy C	1.7
Na	4.9
Al	12.7
K	2.3
Sc	23.6
Ge	6.3
In	19.5
Sn	6.5
Cs	39.3
Gd	6.5
Tb	13.5
Dy	6.5

Author Manuscript:
Published in final edited form as: *Surf. Interface Anal*. Volume 37, Issue 1, Pages 1 - 14 (2005).
https://doi.org/10.1002/sia.1997

Table 7. Values of M_{tot}^2 (for $\Delta E_{\max} = 30$ keV) and $(\rho M_{tot}^2)^{-1}$ for the three allotropes of carbon.

Material	M_{tot}^2	$(\rho M_{tot}^2)^{-1}$ (cm^3 g^{-1})
diamond	1.552	0.183
graphite	2.038	0.218
glassy carbon	1.690	0.329

Author Manuscript:
Published in final edited form as: *Surf. Interface Anal*. Volume 37, Issue 1, Pages 1 - 14 (2005).
https://doi.org/10.1002/sia.1997

Figure Captions

Fig. 1 Plots of the energy loss function, $\mathrm{Im}[-1/\varepsilon(\Delta E)]$, as a function of energy loss, ΔE, for diamond and graphite (from the optical data shown in Table 2).

Fig. 2. Plots of M_{tot}^2 [from Eq. (3)] for diamond and graphite as a function of $\Delta E_{\max}$.

Fig. 3. Plots of Z_{eff} [from Eq. (1)] for diamond and graphite as a function of $\Delta E_{\max}$.

Fig. 4. Plots of P_{eff} [from Eq. (2)] for diamond and graphite as a function of $\Delta E_{\max}$.

Fig. 5. Inelastic mean free paths (solid circles) calculated for lithium as a function of electron energy. IMFP values are shown for the 10 eV to 40 eV range to illustrate trends but these results are not considered to be reliable (see text). The solid line is a fit to the modified Bethe equation [Eq. (4)]; values of the parameters found in the fit are shown in Table 5. The dashed line shows IMFPs calculated from the TPP-2M predictive formula [Eqs. (4) and (6)] using the parameters listed in Table 1.

Fig. 6. IMFP results for beryllium as a function of electron energy; see caption to Fig. 5.

Fig. 7. IMFP results for diamond as a function of electron energy; see caption to Fig. 5.

Fig. 8. IMFP results for graphite as a function of electron energy; see caption to Fig. 5. Measurements of IMFPs by elastic-peak electron spectroscopy from Lesiak *et al*. (ref. 28) and Tanuma *et al*. (ref. 29) are shown as open circles and solid diamonds, respectively.

Fig. 9. IMFP results for glassy carbon (from Ref. 2) as a function of electron energy; see caption to Fig. 5. Measurements of IMFPs by elastic-peak electron spectroscopy from Lesiak *et al*. (ref. 28) are shown as open circles.

Fig. 10. IMFP results for sodium as a function of electron energy; see caption to Fig. 5.

Author Manuscript:
Published in final edited form as: *Surf. Interface Anal*. Volume 37, Issue 1, Pages 1 - 14 (2005).
https://doi.org/10.1002/sia.1997

Fig. 11. IMFP results for aluminum as a function of electron energy; see caption to Fig. 5.

Fig. 12. IMFP results for germanium as a function of electron energy; see caption to Fig. 5.

Fig. 13. IMFP results for indium as a function of electron energy. The long-dashed and short-dashed lines show IMFPs calculated from the TPP-2M equation [Eqs. (4) and (6)] with $N_v = 3$ and $N_v = 13$, respectively. See also caption to Fig. 5.

Fig. 14. IMFP results for tin as a function of electron energy. The long-dashed and short-dashed lines show IMFPs calculated from the TPP-2M equation [Eqs. (4) and (6)] with $N_v = 4$ and $N_v = 14$, respectively. See also caption to Fig. 5.

Fig. 15. IMFP results for cesium as a function of electron energy. The long-dashed, dot-dashed, and short-dashed lines show IMFPs calculated from the TPP-2M equation [Eqs. (4) and (6)] with $N_v = 1$, $N_v = 7$, and $N_v = 9$, respectively. See also caption to Fig. 5.

Fig. 16. The solid circles show values of β, β_{obs}, found from fits of Eq. (4) to the calculated IMFPs for groups of elements, inorganic compounds, and organic compounds as a function of $(E_p^2 + E_g^2)^{-0.5}$. The long-dashed and short-dashed lines are plots of Eq. 6(a) with $\rho = 1$ g/cm^3 and $\rho = 10$ g/cm^3, respectively.

Fig. 17. Values of $\beta_r = \beta_{obs} - 0.944(E_p^2 + E_g^2)^{-0.5}$ (solid circles) as a function of density. The solid line is a plot of $\beta_r = -0.10 + 0.069\,\rho^{0.1}$, the variation expected from Eq. 6(a).

Fig. 18. Values of β from Eq. 6(a) (solid circles) versus β_{obs}. The dashed line is a plot of $\beta = \beta_{obs}$.

Fig. 19. Plot of (a) the energy loss spectrum of Gd versus energy loss ΔE for energy losses up to 200 eV, (b) Z_{eff} versus ΔE_{max} for Gd from Eq. (1), and (c) M_{tot}^2 versus ΔE_{max} for Gd from Eq. (3).

Author Manuscript:
Published in final edited form as: *Surf. Interface Anal*. Volume 37, Issue 1, Pages 1 - 14 (2005).
https://doi.org/10.1002/sia.1997

Fig. 20. Plot of (a) the energy loss spectrum of Cs versus energy loss ΔE for energy losses up to 200 eV, (b) Z_{eff} versus $\Delta E_{\max}$ for Cs from Eq. (1), and (c) M_{tot}^2 versus $\Delta E_{\max}$ for Cs from Eq. (3).

Fig. 21. Plot of (a) the energy loss spectrum of Sn versus energy loss ΔE for energy losses up to 200 eV, (b) Z_{eff} versus $\Delta E_{\max}$ for Sn from Eq. (1), and (c) M_{tot}^2 versus $\Delta E_{\max}$ for Sn from Eq. (3).

Author Manuscript:
Published in final edited form as: *Surf. Interface Anal*. Volume 37, Issue 1, Pages 1 - 14 (2005).
https://doi.org/10.1002/sia.1997

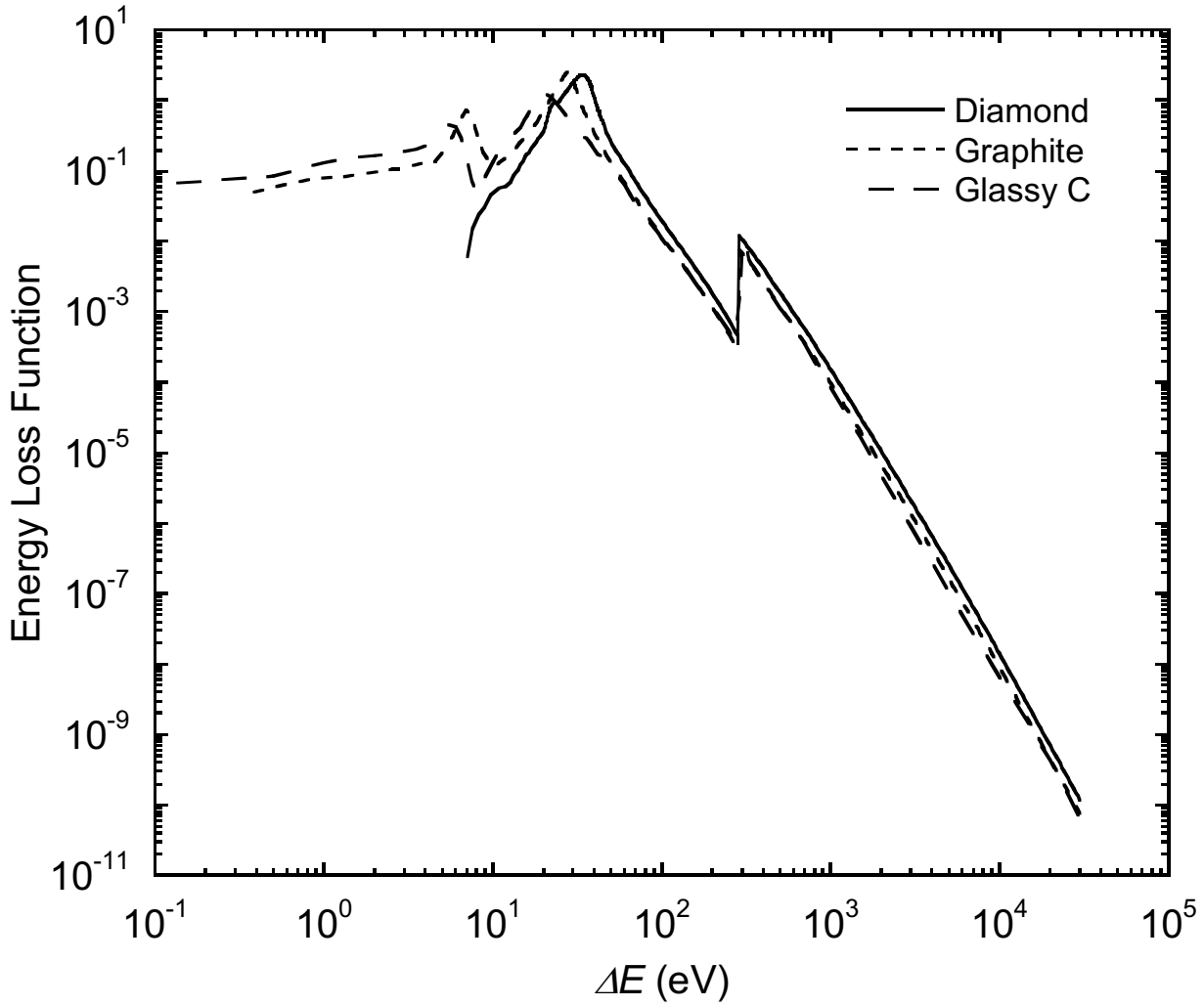

Fig. 1.

Author Manuscript:
Published in final edited form as: *Surf. Interface Anal*. Volume 37, Issue 1, Pages 1 - 14 (2005).
https://doi.org/10.1002/sia.1997

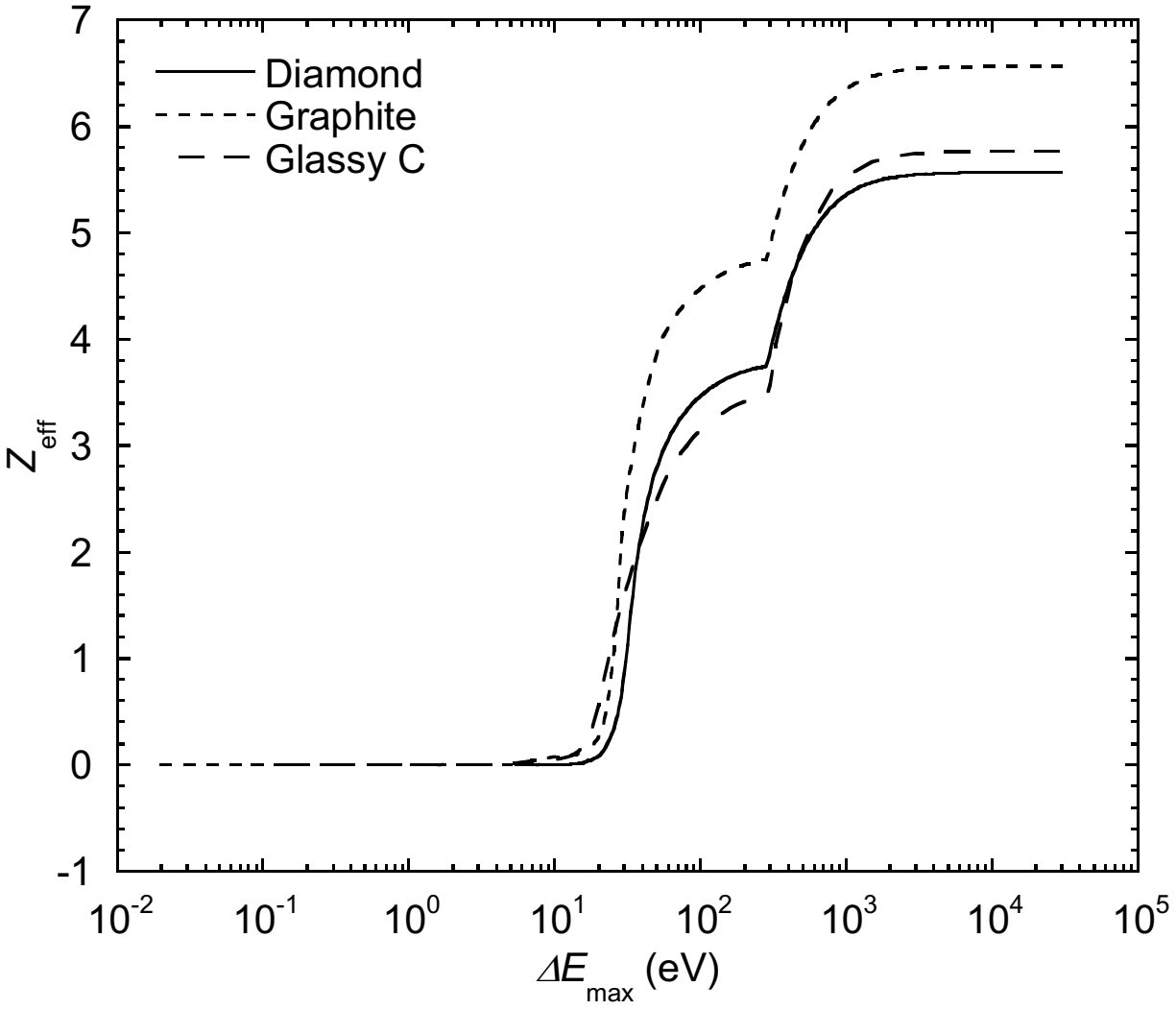

Fig. 2.

Author Manuscript:
Published in final edited form as: *Surf. Interface Anal*. Volume 37, Issue 1, Pages 1 - 14 (2005).
https://doi.org/10.1002/sia.1997

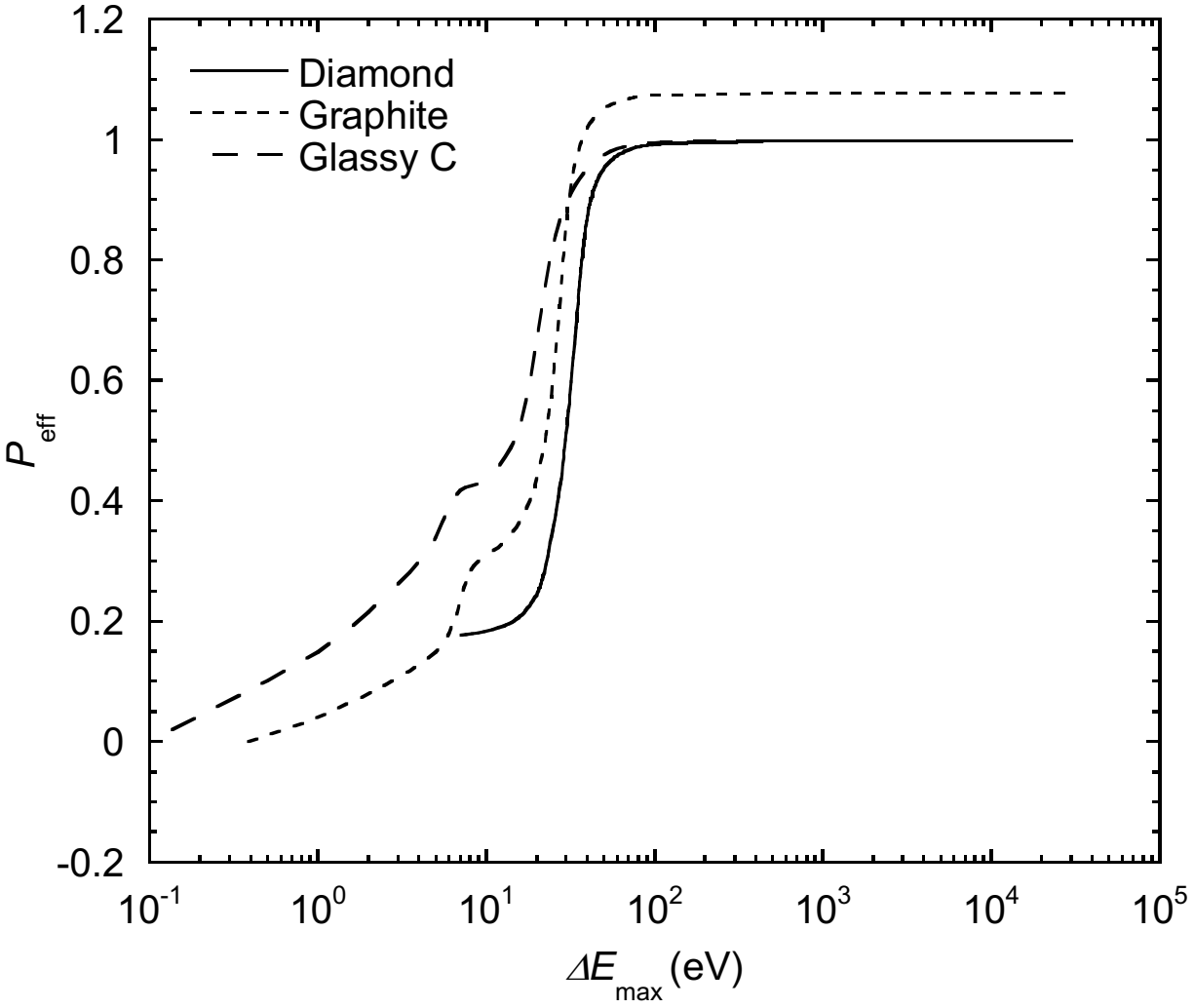

Fig. 3.

Author Manuscript:
Published in final edited form as: *Surf. Interface Anal*. Volume 37, Issue 1, Pages 1 - 14 (2005).
https://doi.org/10.1002/sia.1997

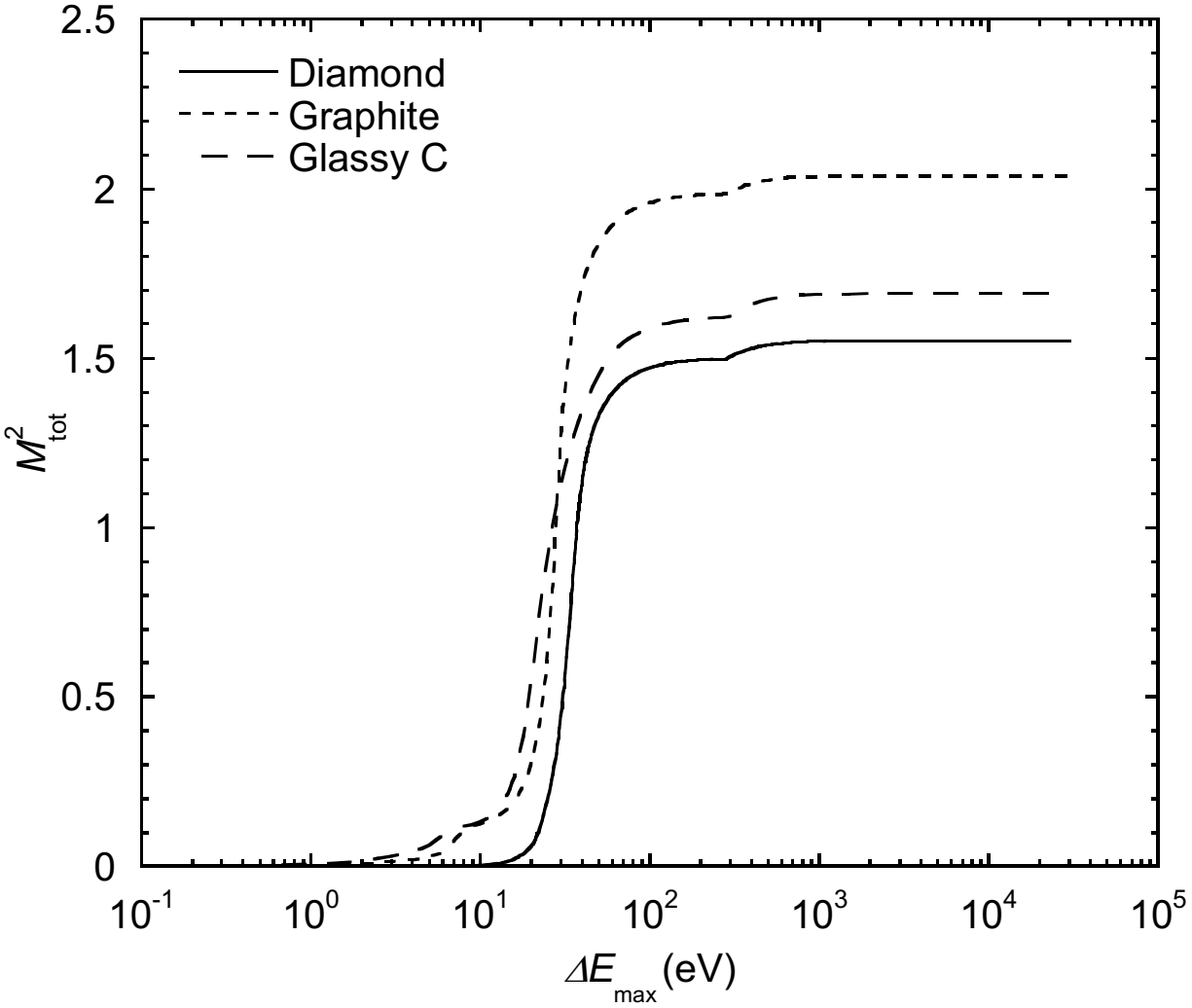

Fig. 4.

Author Manuscript:
Published in final edited form as: *Surf. Interface Anal*. Volume 37, Issue 1, Pages 1 - 14 (2005).
https://doi.org/10.1002/sia.1997

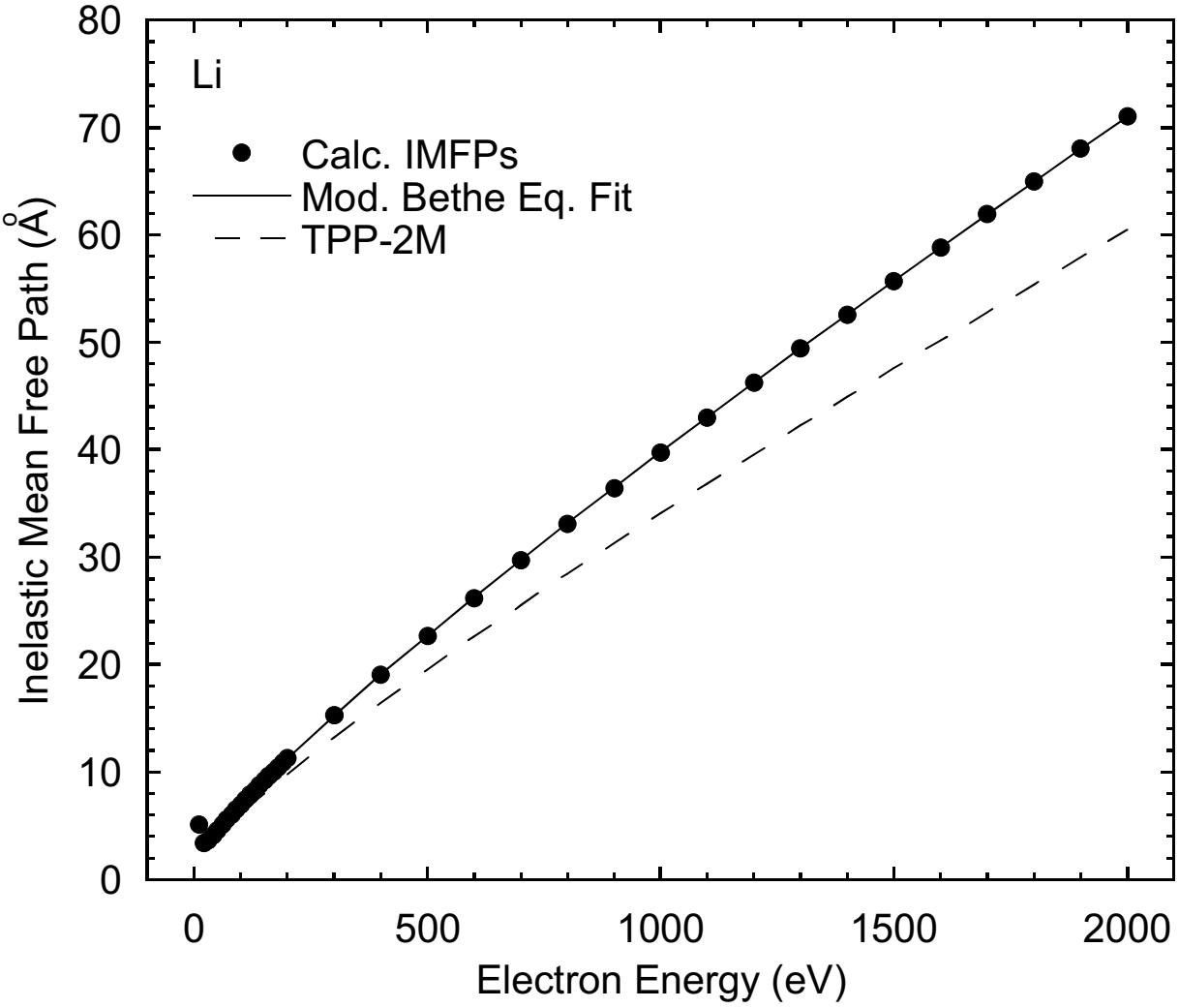

Fig. 5.

Author Manuscript:
Published in final edited form as: *Surf. Interface Anal*. Volume 37, Issue 1, Pages 1 - 14 (2005).
https://doi.org/10.1002/sia.1997

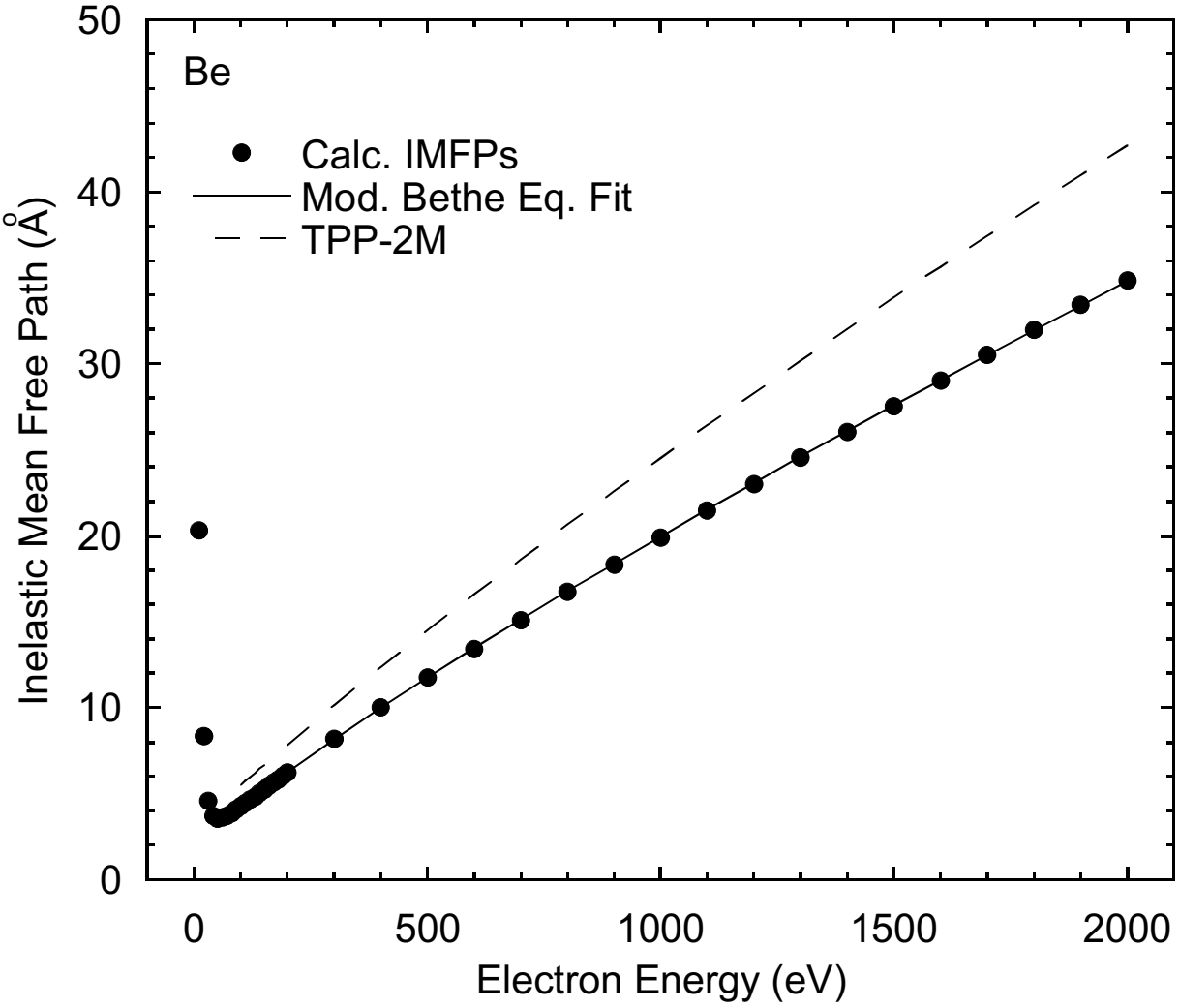

Fig. 6.

Author Manuscript:
Published in final edited form as: *Surf. Interface Anal*. Volume 37, Issue 1, Pages 1 - 14 (2005).
https://doi.org/10.1002/sia.1997

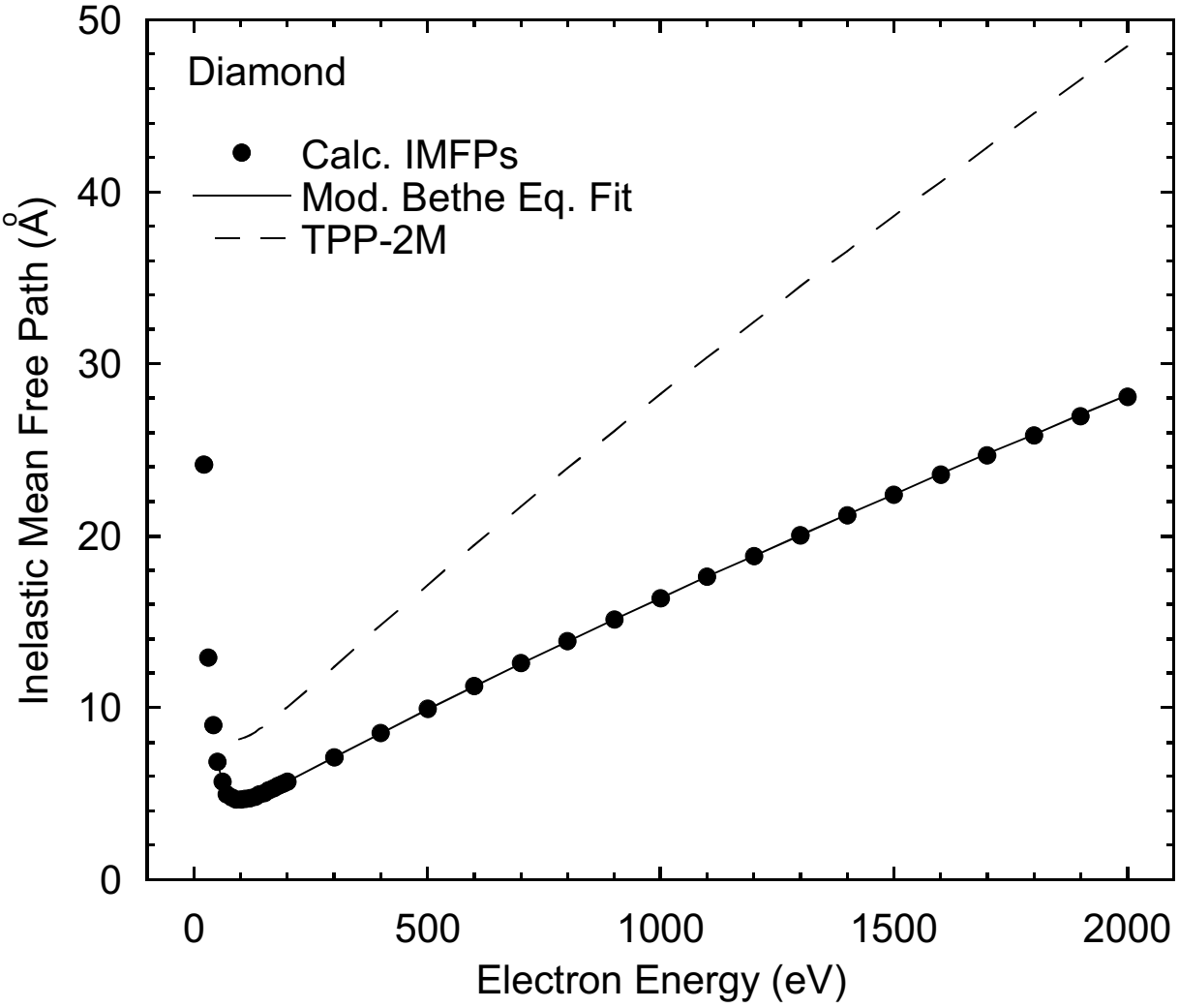

Fig. 7.

Author Manuscript:
Published in final edited form as: *Surf. Interface Anal*. Volume 37, Issue 1, Pages 1 - 14 (2005).
https://doi.org/10.1002/sia.1997

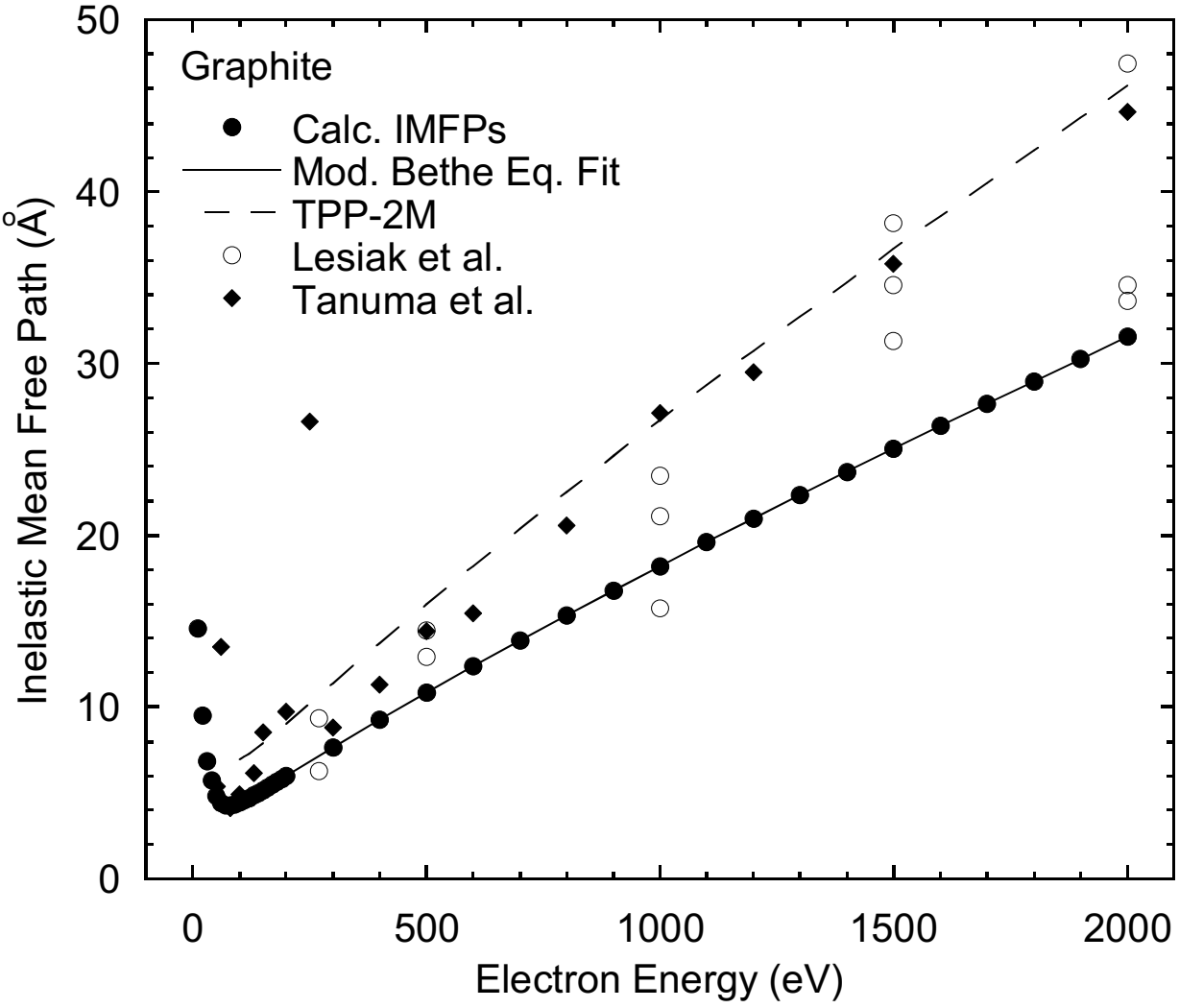

Fig. 8.

Author Manuscript:
Published in final edited form as: *Surf. Interface Anal*. Volume 37, Issue 1, Pages 1 - 14 (2005).
https://doi.org/10.1002/sia.1997

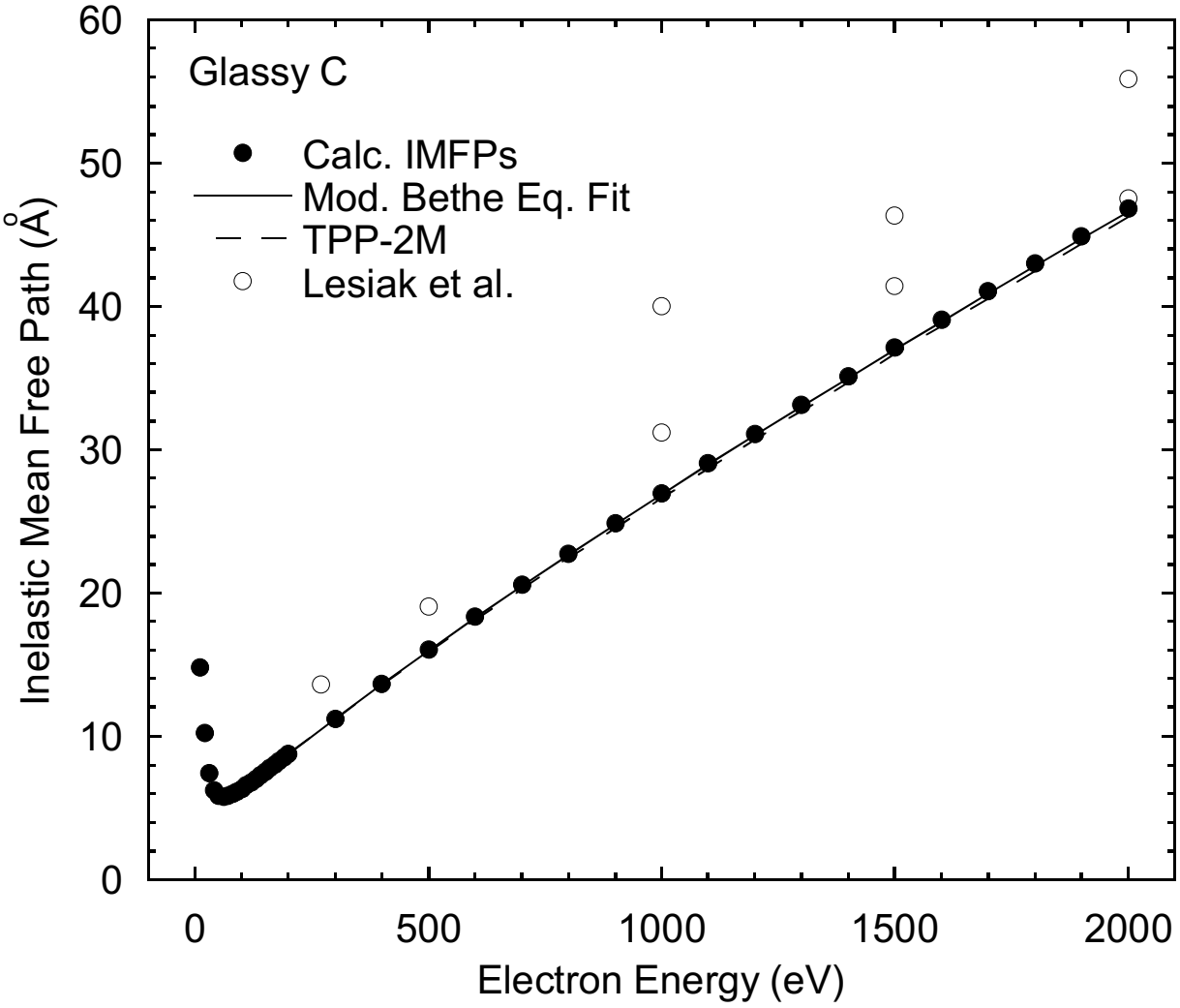

Fig. 9.

Author Manuscript:
Published in final edited form as: *Surf. Interface Anal*. Volume 37, Issue 1, Pages 1 - 14 (2005).
https://doi.org/10.1002/sia.1997

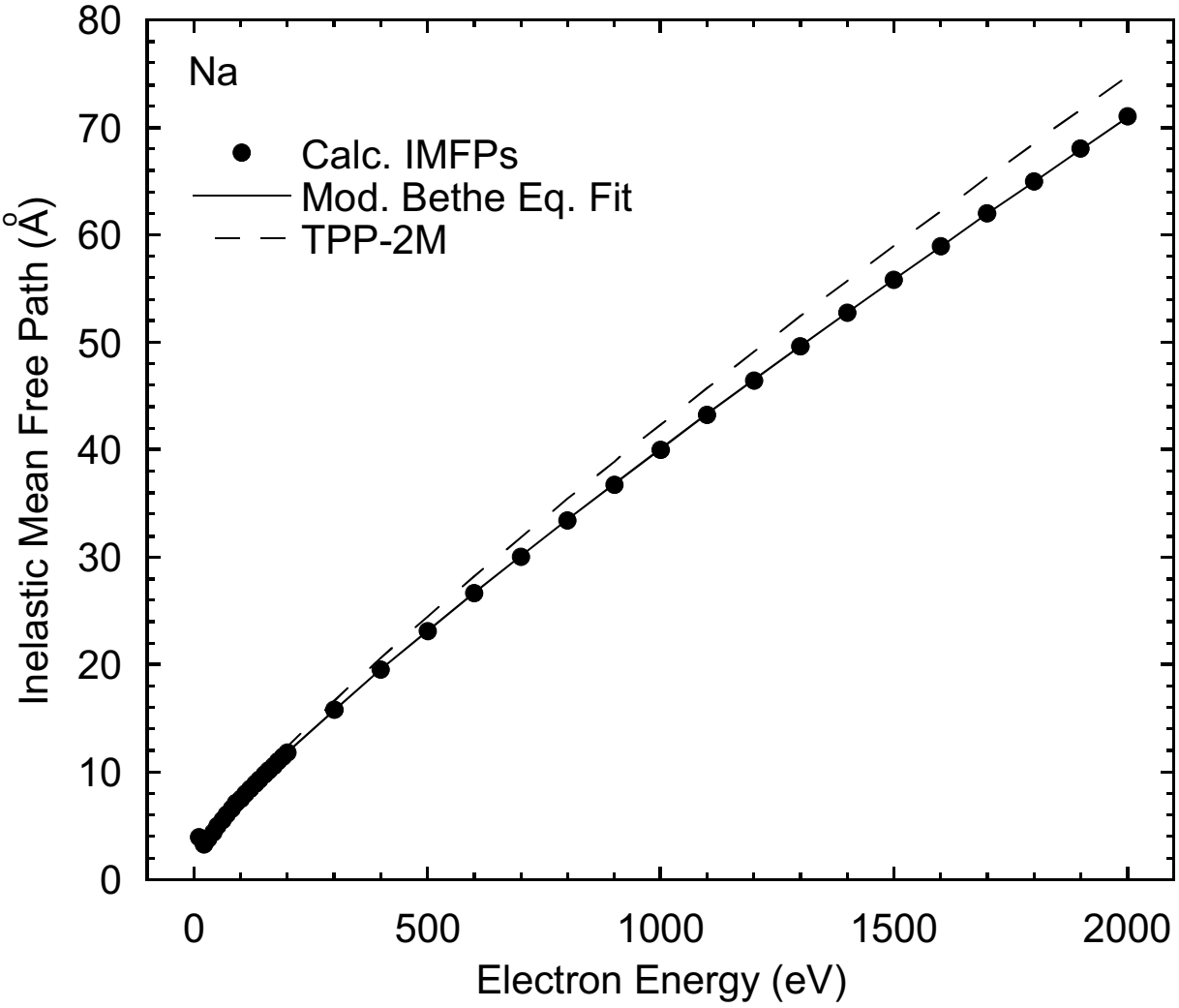

Fig. 10.

Author Manuscript:
Published in final edited form as: *Surf. Interface Anal*. Volume 37, Issue 1, Pages 1 - 14 (2005).
https://doi.org/10.1002/sia.1997

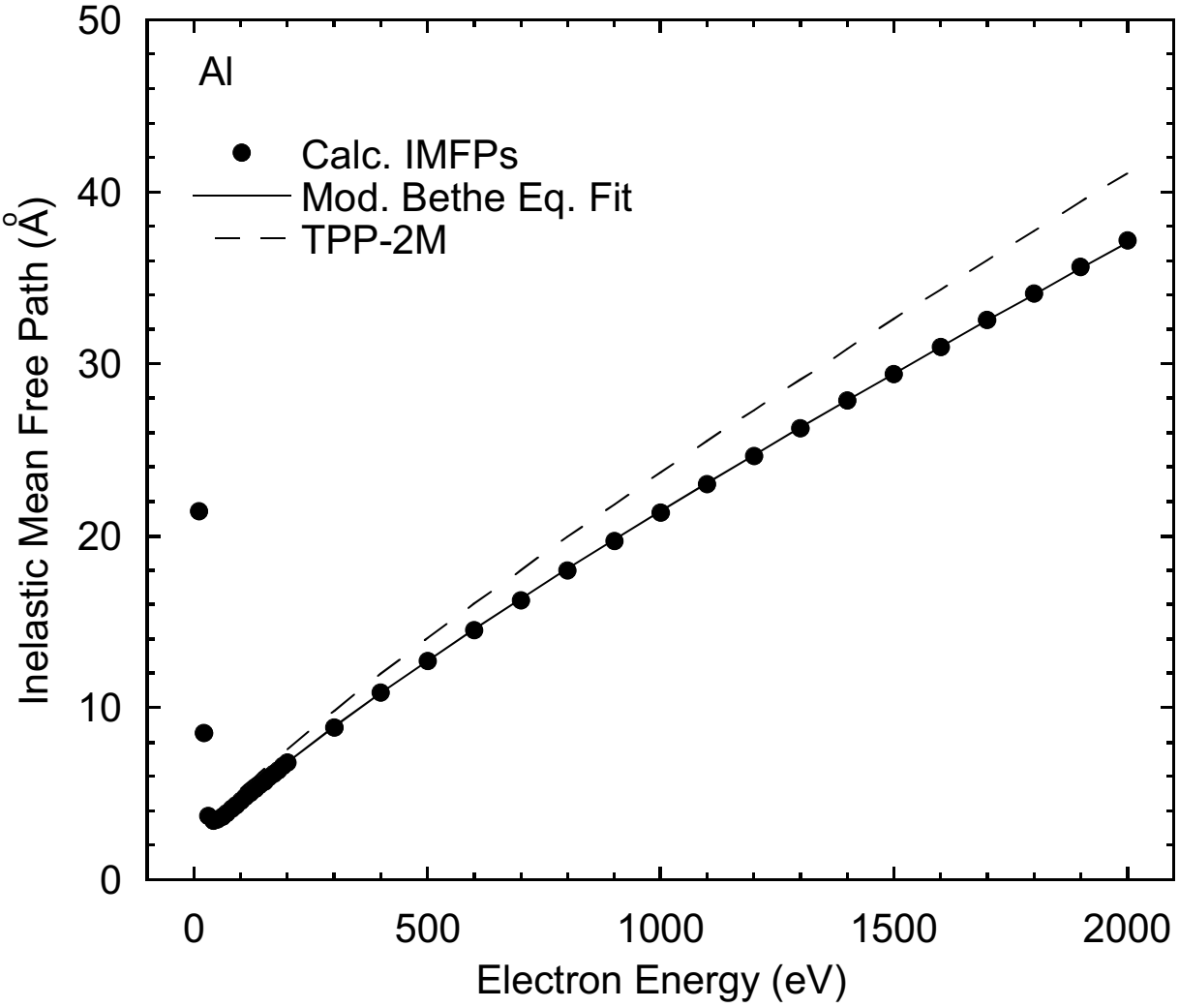

Fig. 11.

Author Manuscript:
Published in final edited form as: *Surf. Interface Anal*. Volume 37, Issue 1, Pages 1 - 14 (2005).
https://doi.org/10.1002/sia.1997

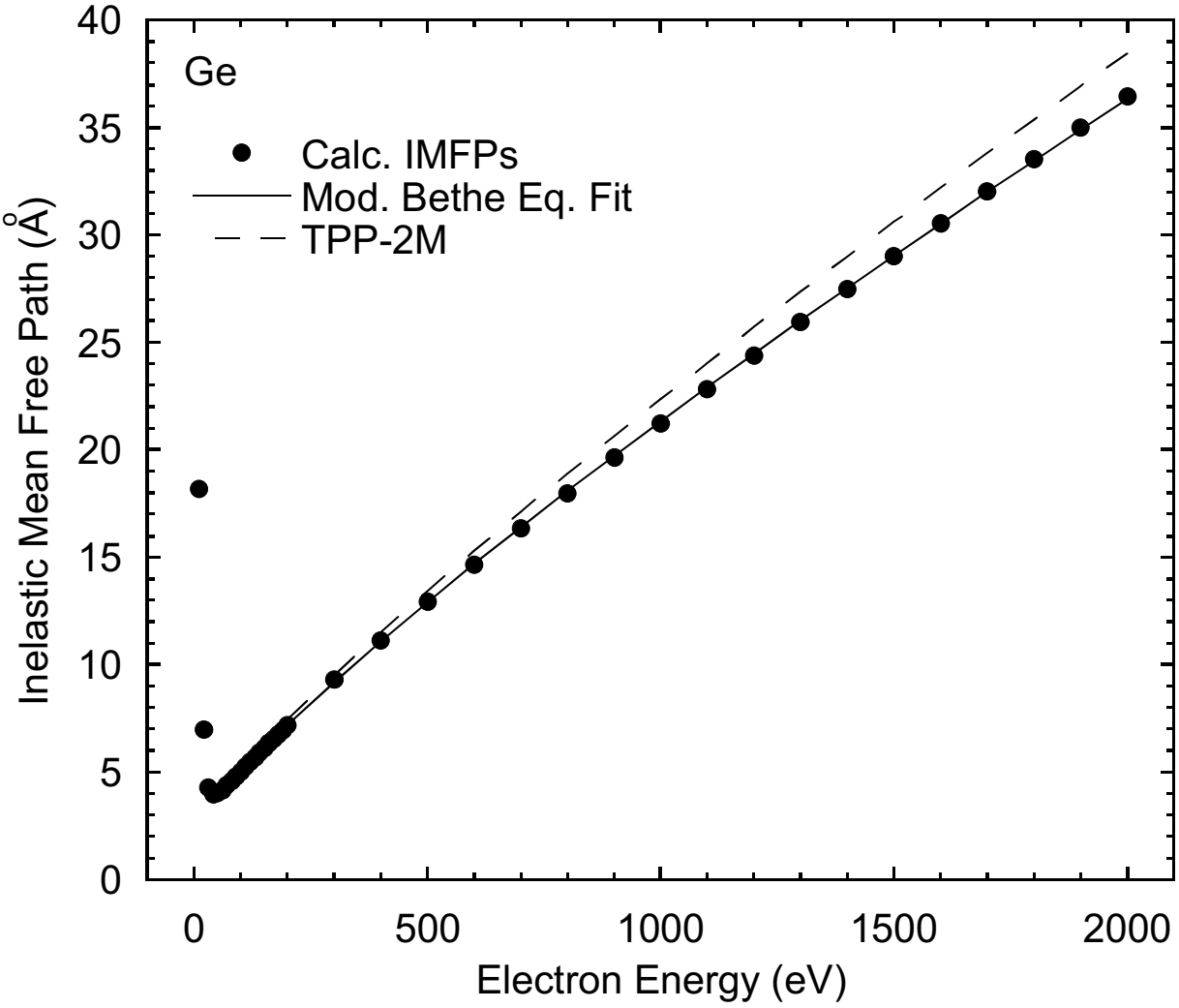

Fig. 12.

Author Manuscript:
Published in final edited form as: *Surf. Interface Anal*. Volume 37, Issue 1, Pages 1 - 14 (2005).
https://doi.org/10.1002/sia.1997

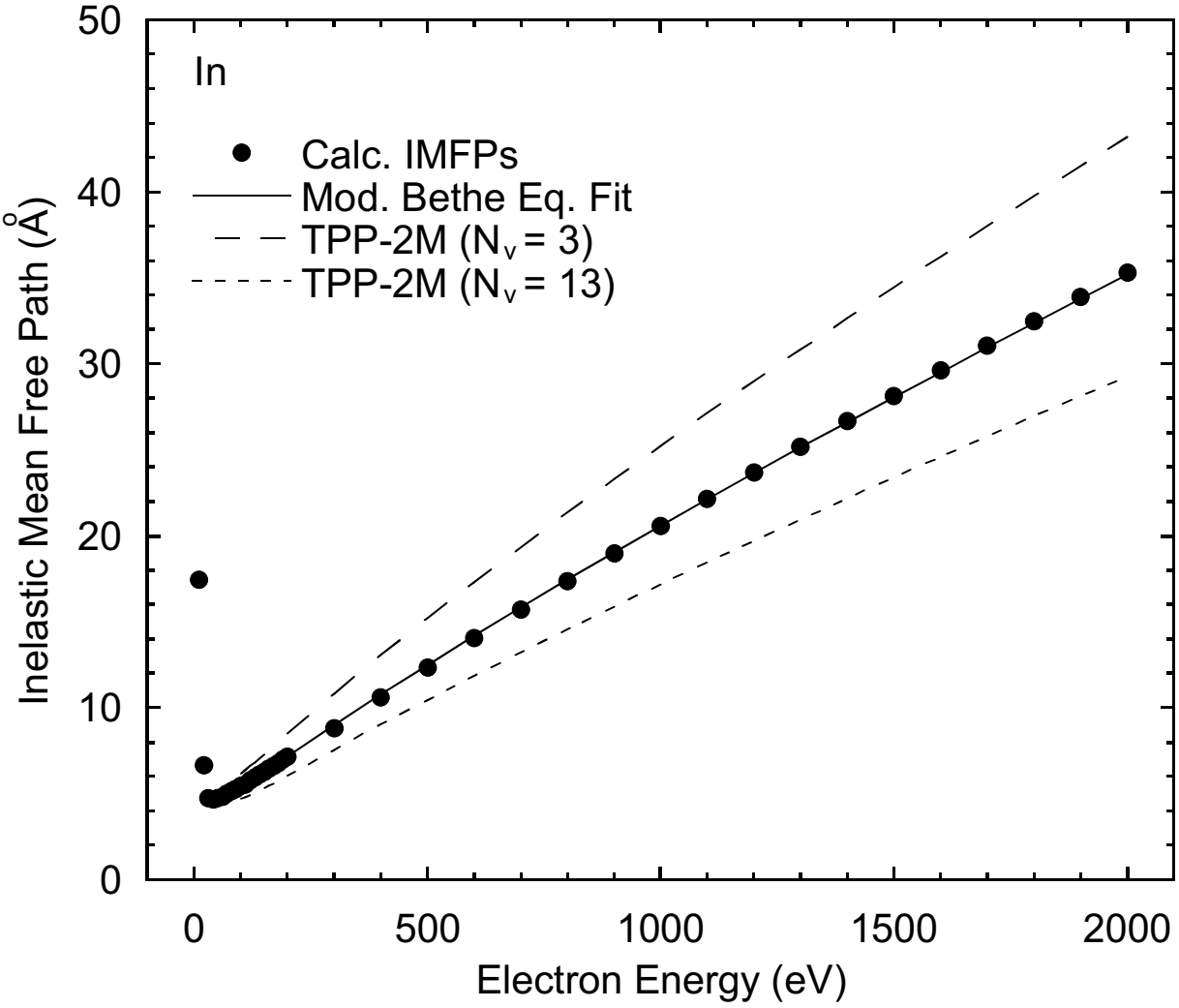

Fig. 13.

Author Manuscript:
Published in final edited form as: *Surf. Interface Anal*. Volume 37, Issue 1, Pages 1 - 14 (2005).
https://doi.org/10.1002/sia.1997

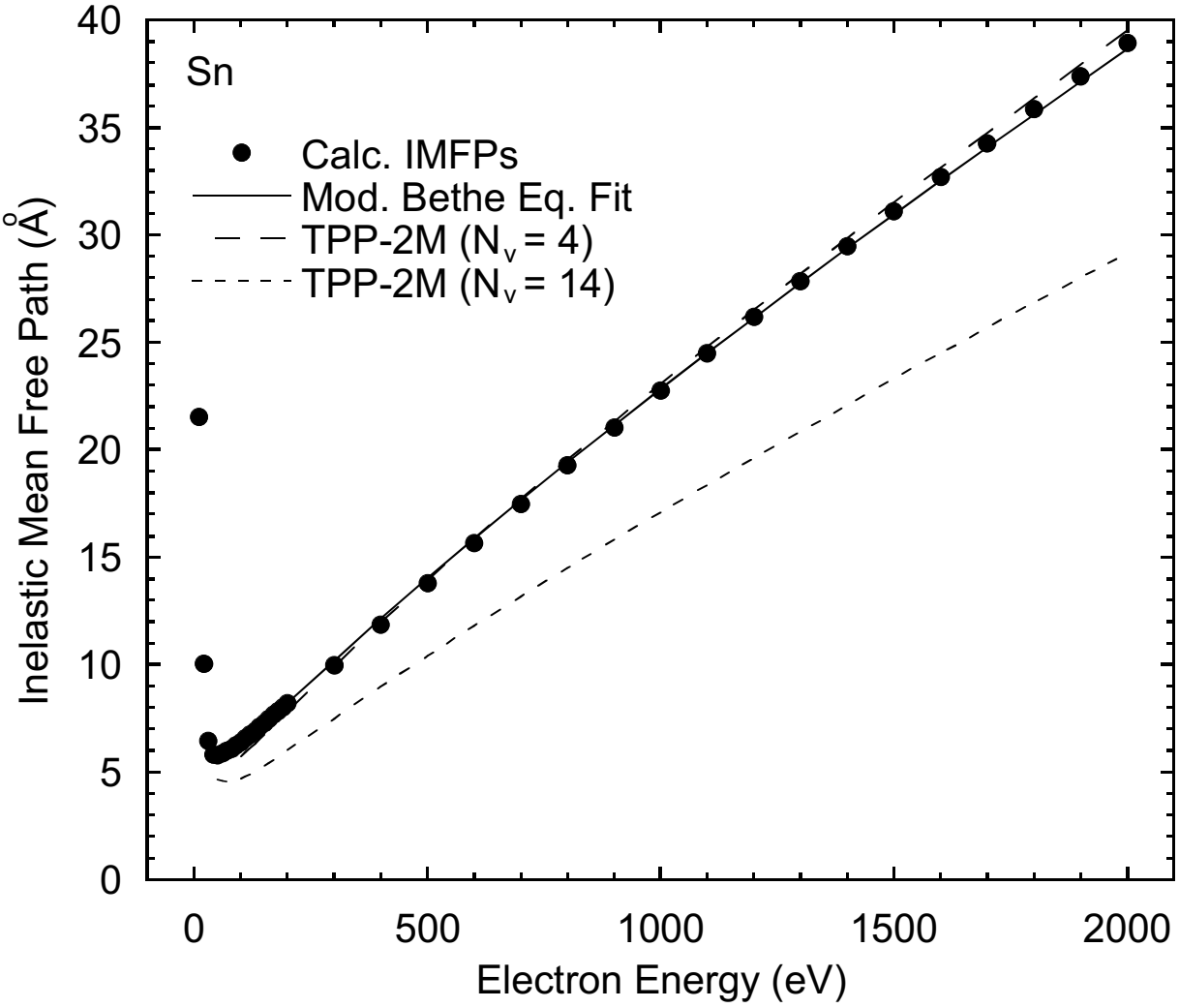

Fig. 14.

Author Manuscript:
Published in final edited form as: *Surf. Interface Anal*. Volume 37, Issue 1, Pages 1 - 14 (2005).
https://doi.org/10.1002/sia.1997

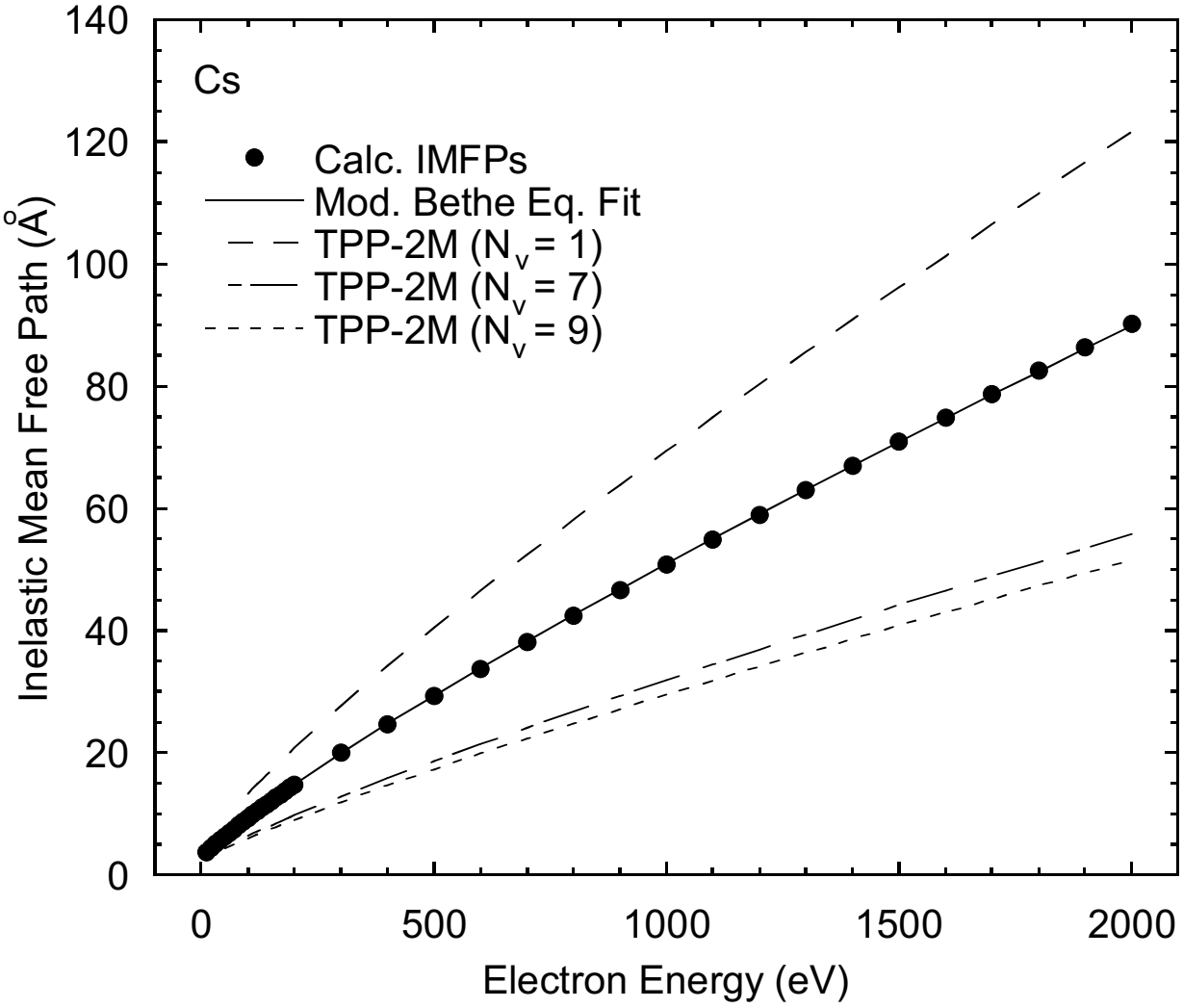

Fig. 15.

Author Manuscript:
Published in final edited form as: *Surf. Interface Anal*. Volume 37, Issue 1, Pages 1 - 14 (2005).
https://doi.org/10.1002/sia.1997

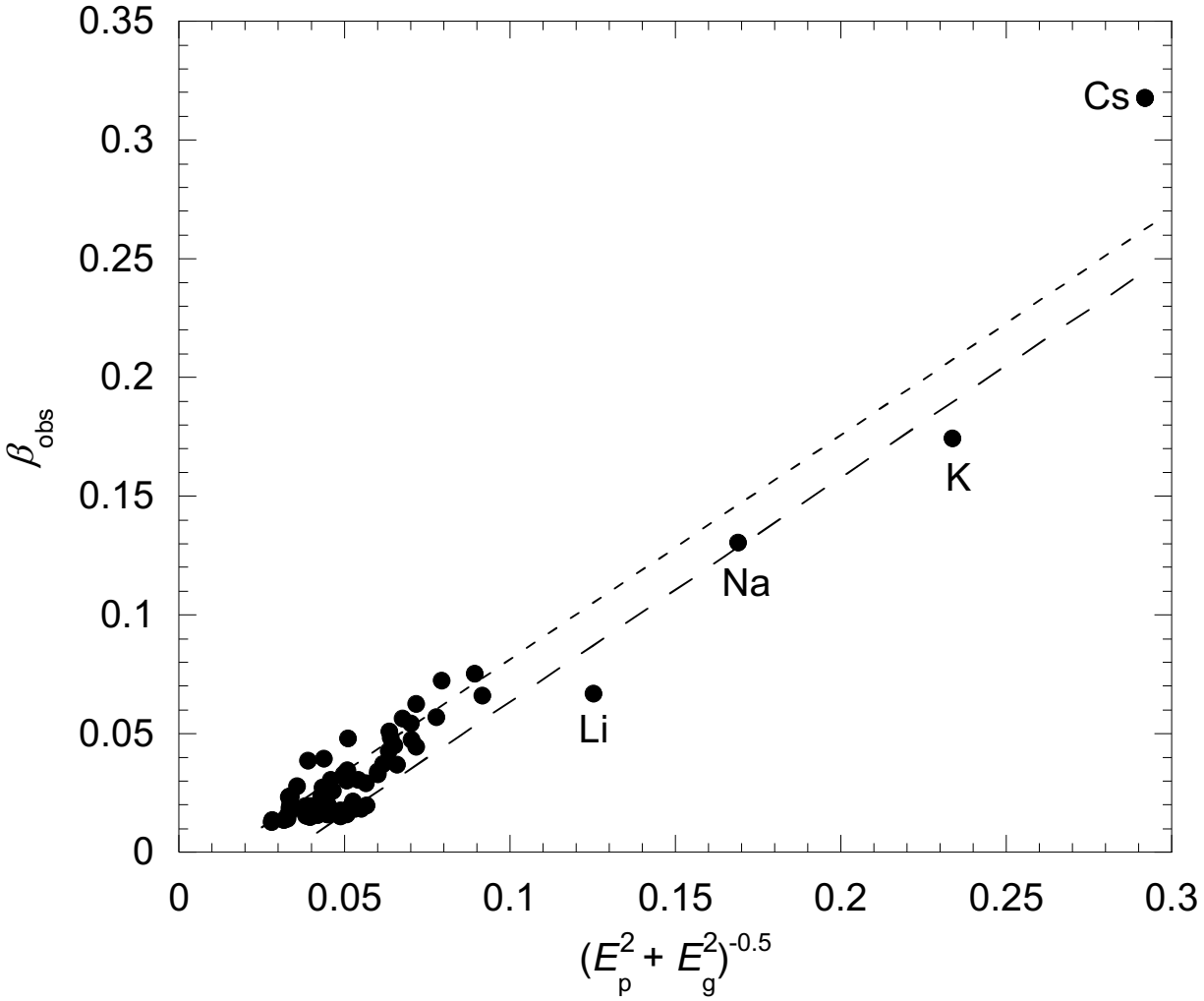

Fig. 16.

Author Manuscript:
Published in final edited form as: *Surf. Interface Anal*. Volume 37, Issue 1, Pages 1 - 14 (2005).
https://doi.org/10.1002/sia.1997

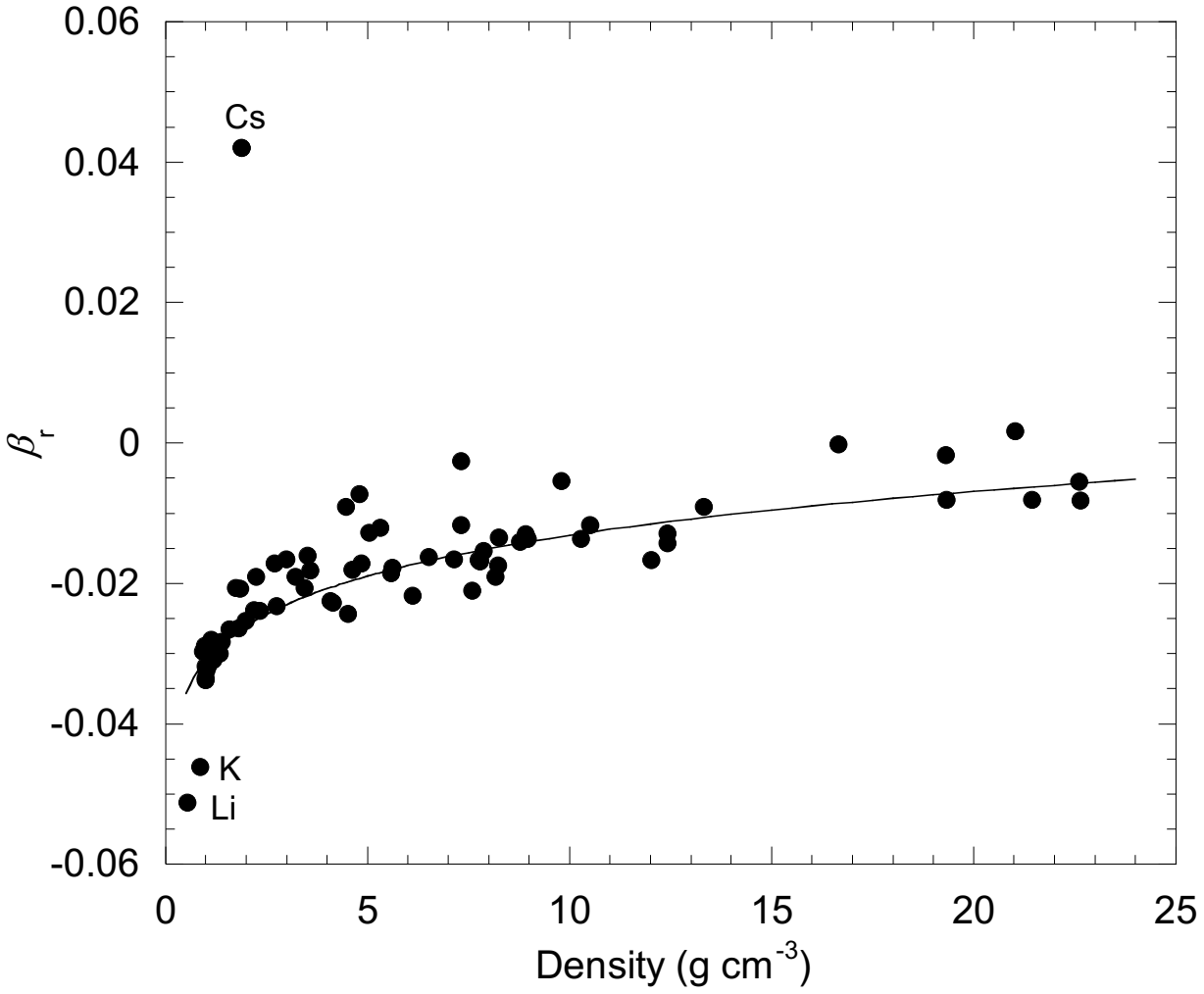

Fig. 17.

Author Manuscript:
Published in final edited form as: *Surf. Interface Anal*. Volume 37, Issue 1, Pages 1 - 14 (2005).
https://doi.org/10.1002/sia.1997

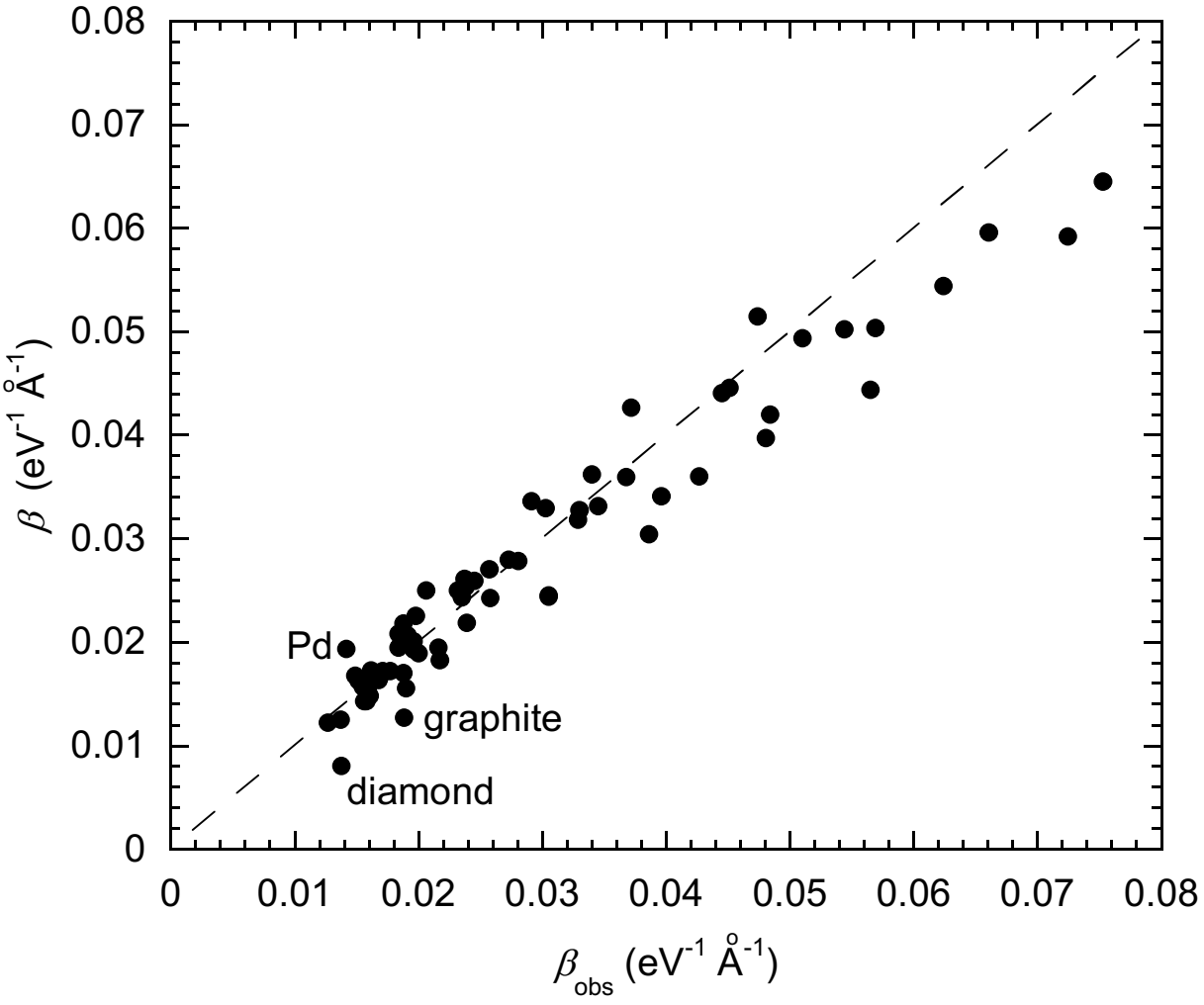

Fig. 18(a).

Author Manuscript:
Published in final edited form as: *Surf. Interface Anal*. Volume 37, Issue 1, Pages 1 - 14 (2005).
https://doi.org/10.1002/sia.1997

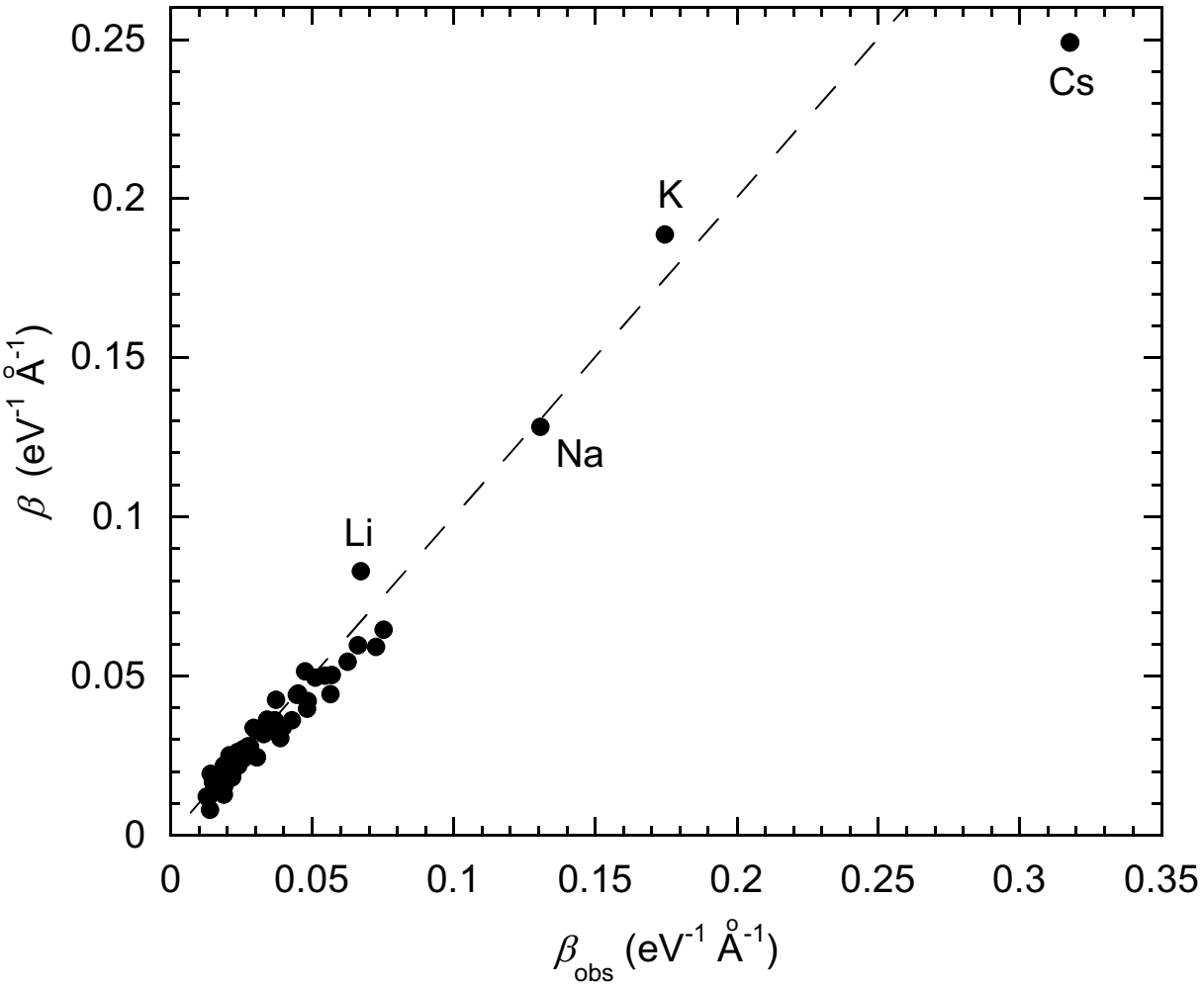

Fig. 18(b).

Author Manuscript:
Published in final edited form as: *Surf. Interface Anal*. Volume 37, Issue 1, Pages 1 - 14 (2005).
https://doi.org/10.1002/sia.1997

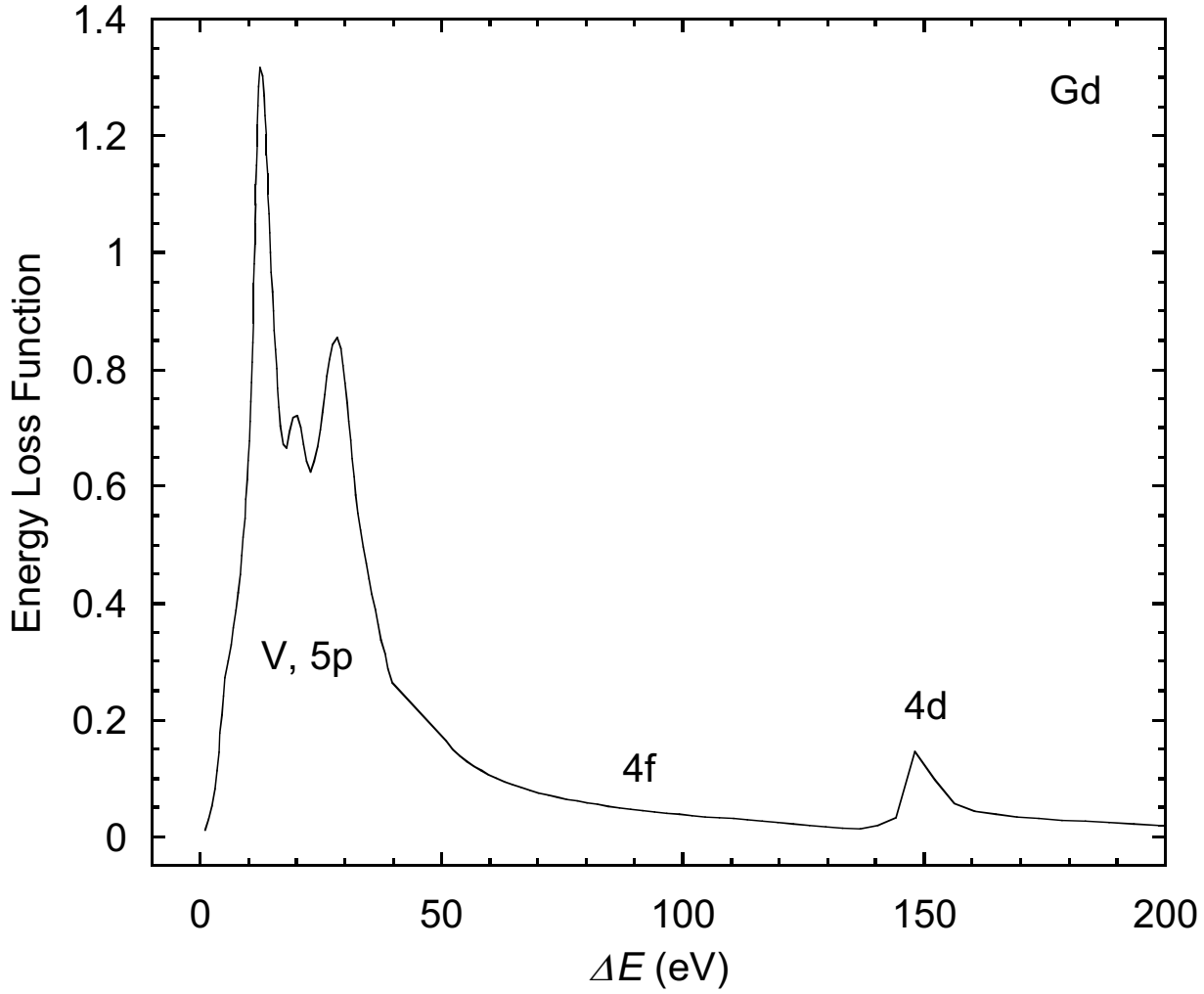

Fig. 19(a).

Author Manuscript:
Published in final edited form as: *Surf. Interface Anal*. Volume 37, Issue 1, Pages 1 - 14 (2005).
https://doi.org/10.1002/sia.1997

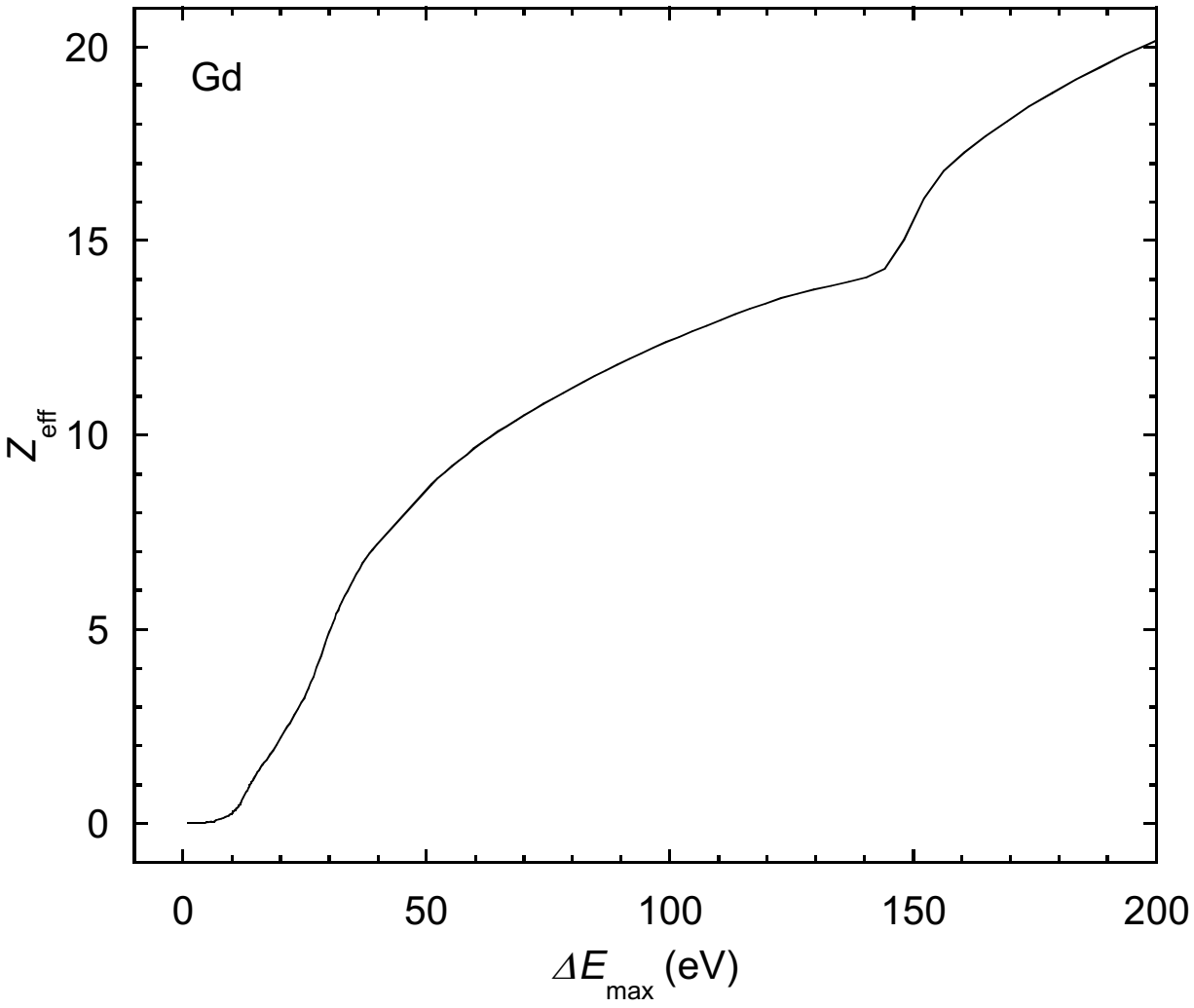

Fig. 19(b).

Author Manuscript:
Published in final edited form as: *Surf. Interface Anal*. Volume 37, Issue 1, Pages 1 - 14 (2005).
https://doi.org/10.1002/sia.1997

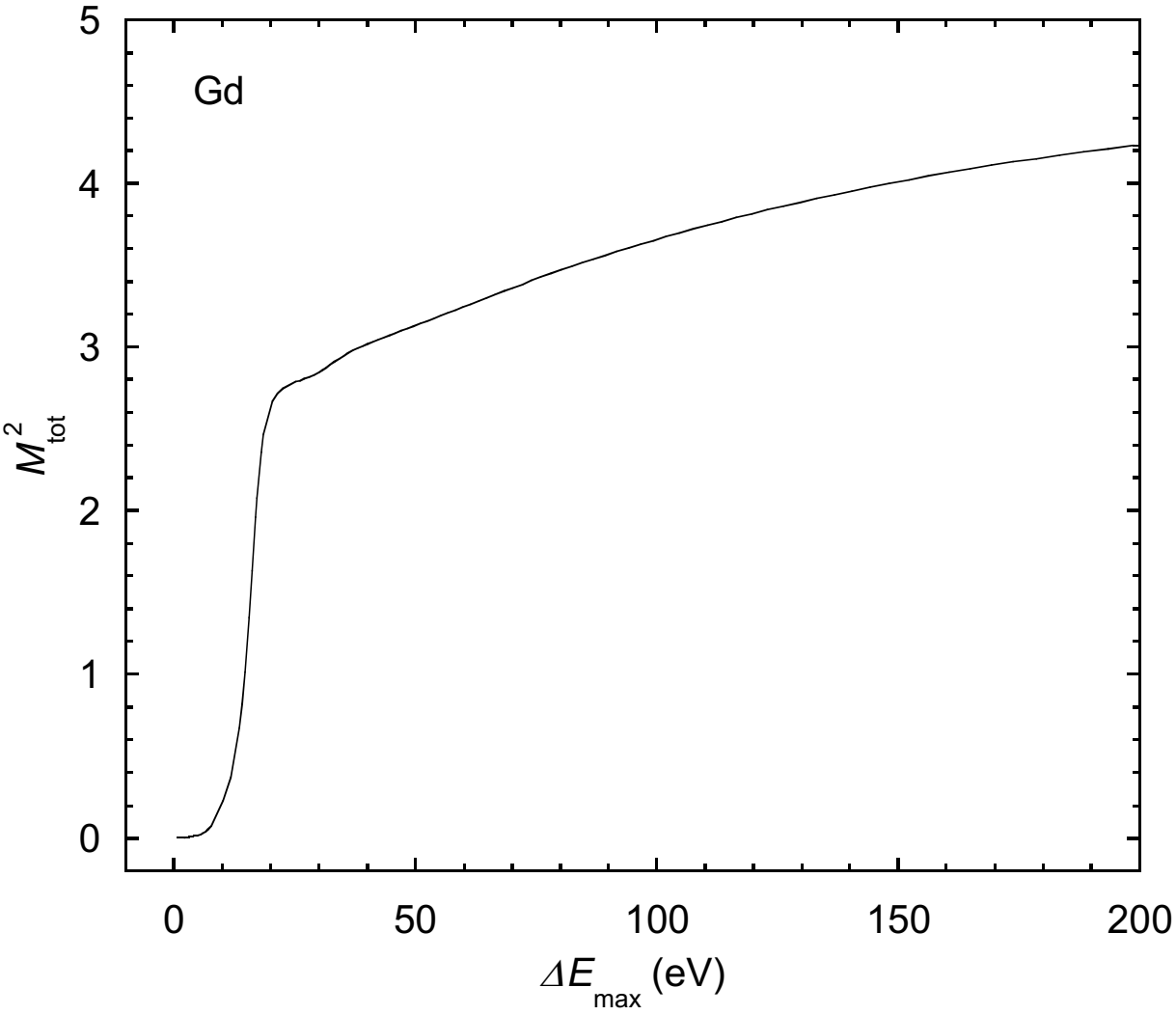

Fig. 19(c).

Author Manuscript:
Published in final edited form as: *Surf. Interface Anal*. Volume 37, Issue 1, Pages 1 - 14 (2005).
https://doi.org/10.1002/sia.1997

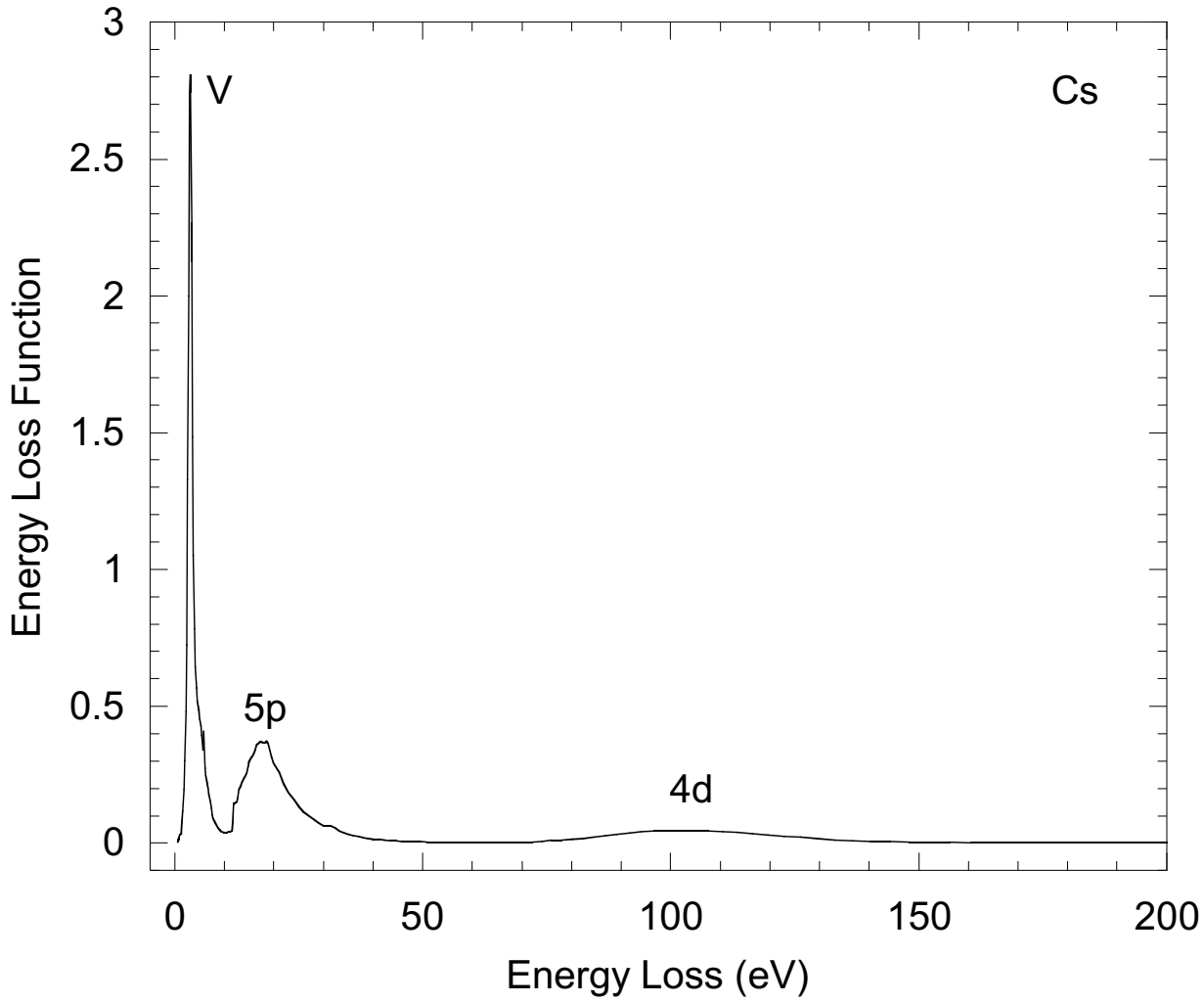

Fig. 20(a).

Author Manuscript:
Published in final edited form as: *Surf. Interface Anal*. Volume 37, Issue 1, Pages 1 - 14 (2005).
https://doi.org/10.1002/sia.1997

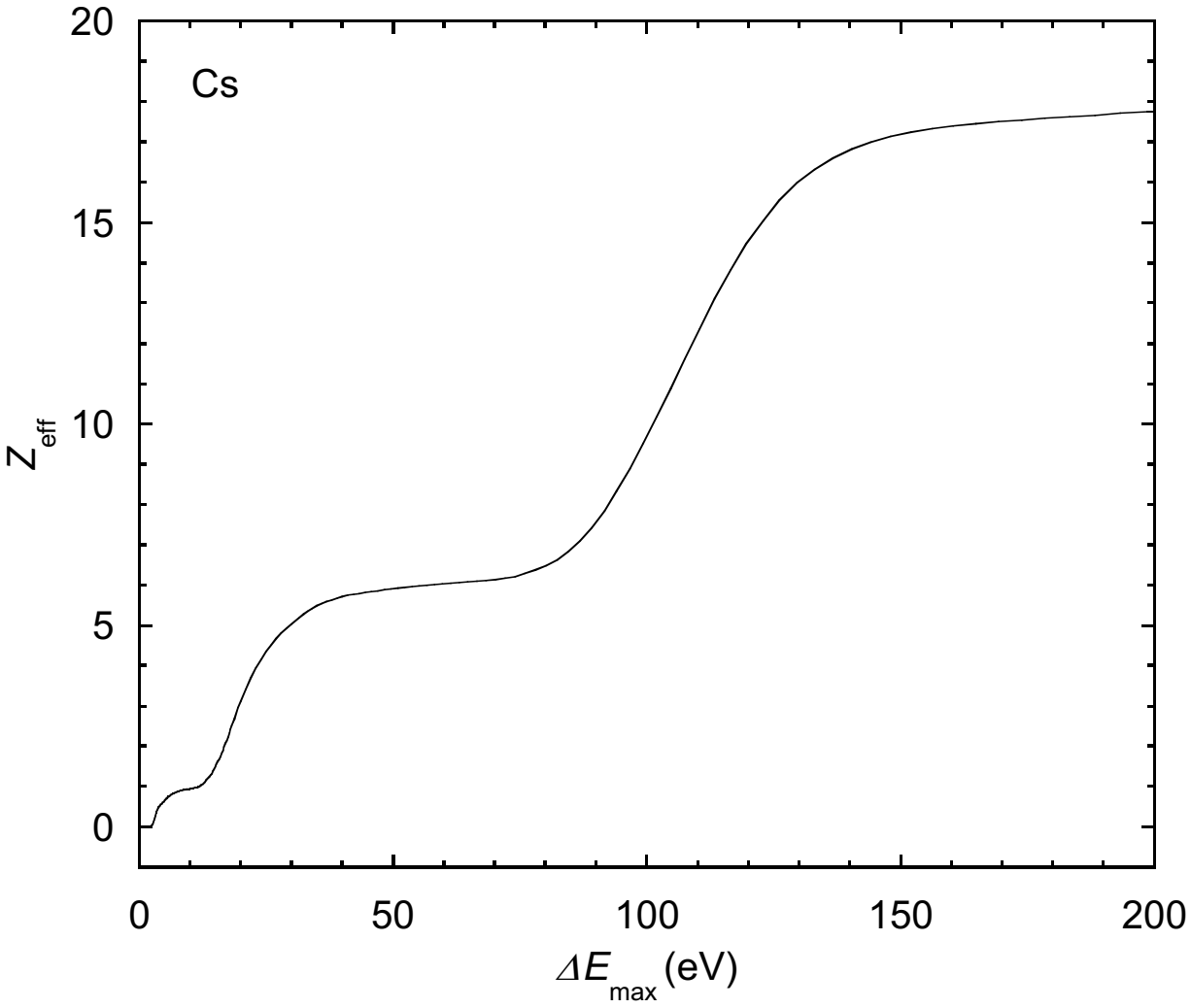

Fig. 20(b).

Author Manuscript:
Published in final edited form as: *Surf. Interface Anal*. Volume 37, Issue 1, Pages 1 - 14 (2005).
https://doi.org/10.1002/sia.1997

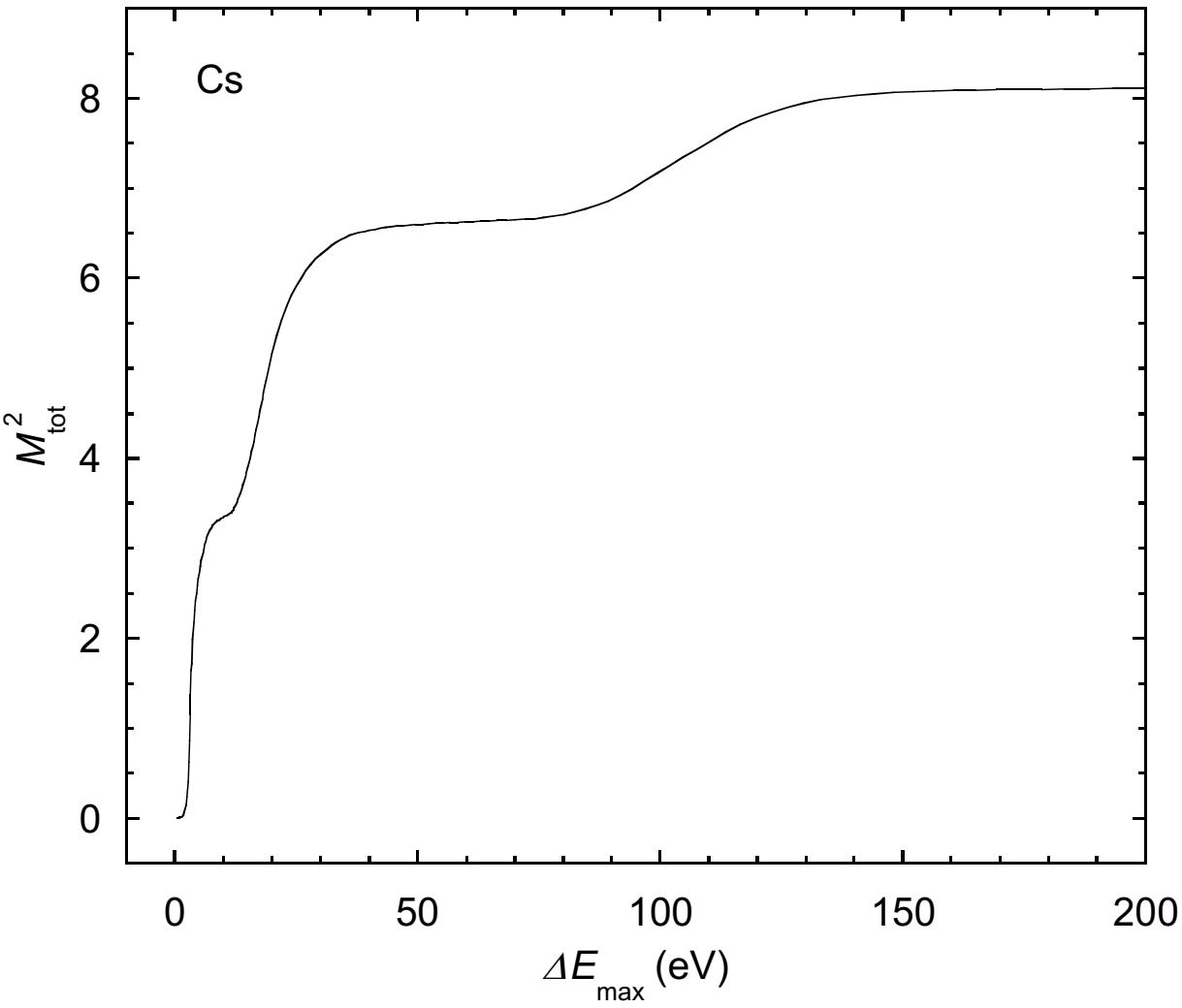

Fig. 20(c).

Author Manuscript:
Published in final edited form as: *Surf. Interface Anal*. Volume 37, Issue 1, Pages 1 - 14 (2005).
https://doi.org/10.1002/sia.1997

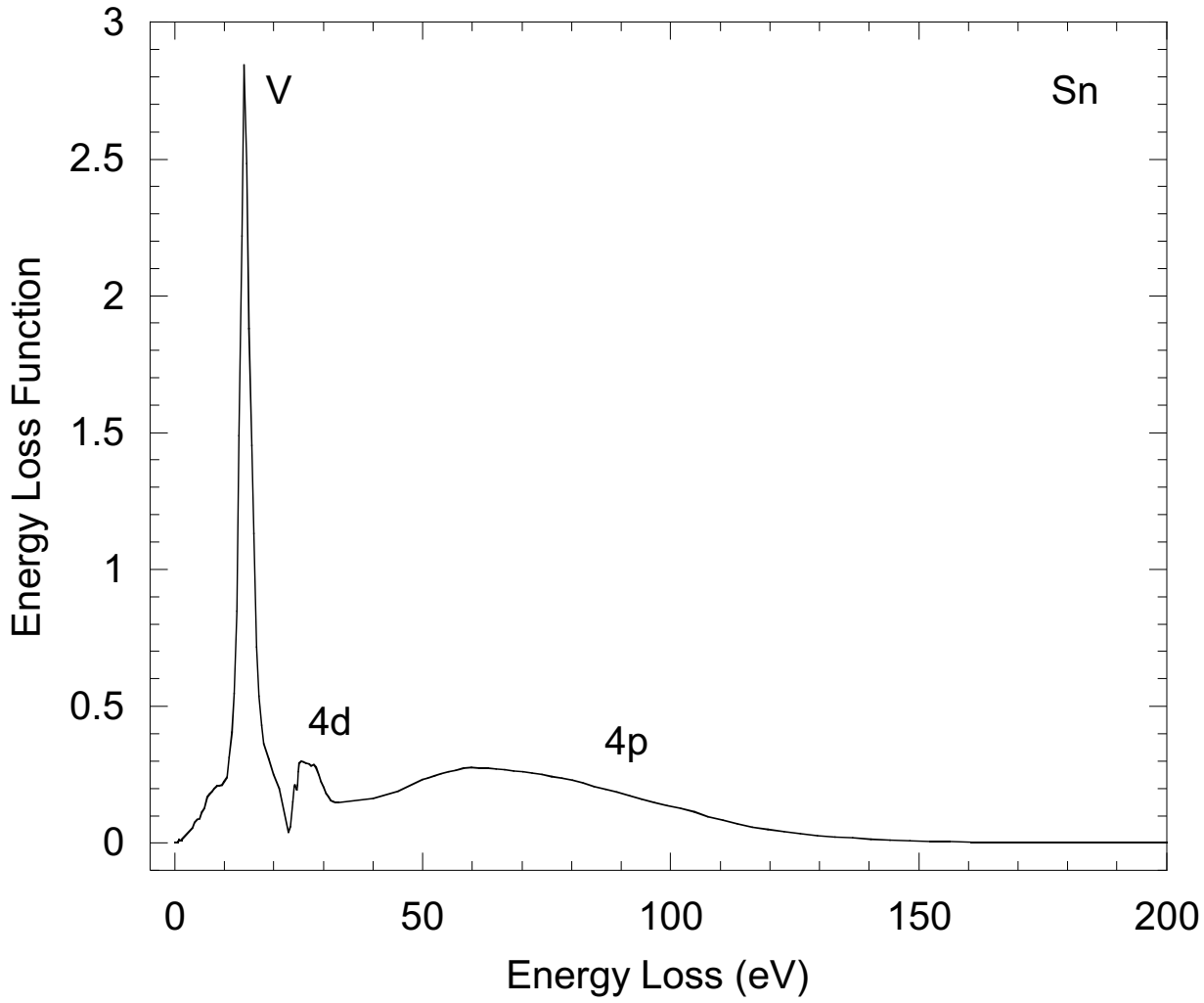

Fig. 21(a).

Author Manuscript:
Published in final edited form as: *Surf. Interface Anal*. Volume 37, Issue 1, Pages 1 - 14 (2005).
https://doi.org/10.1002/sia.1997

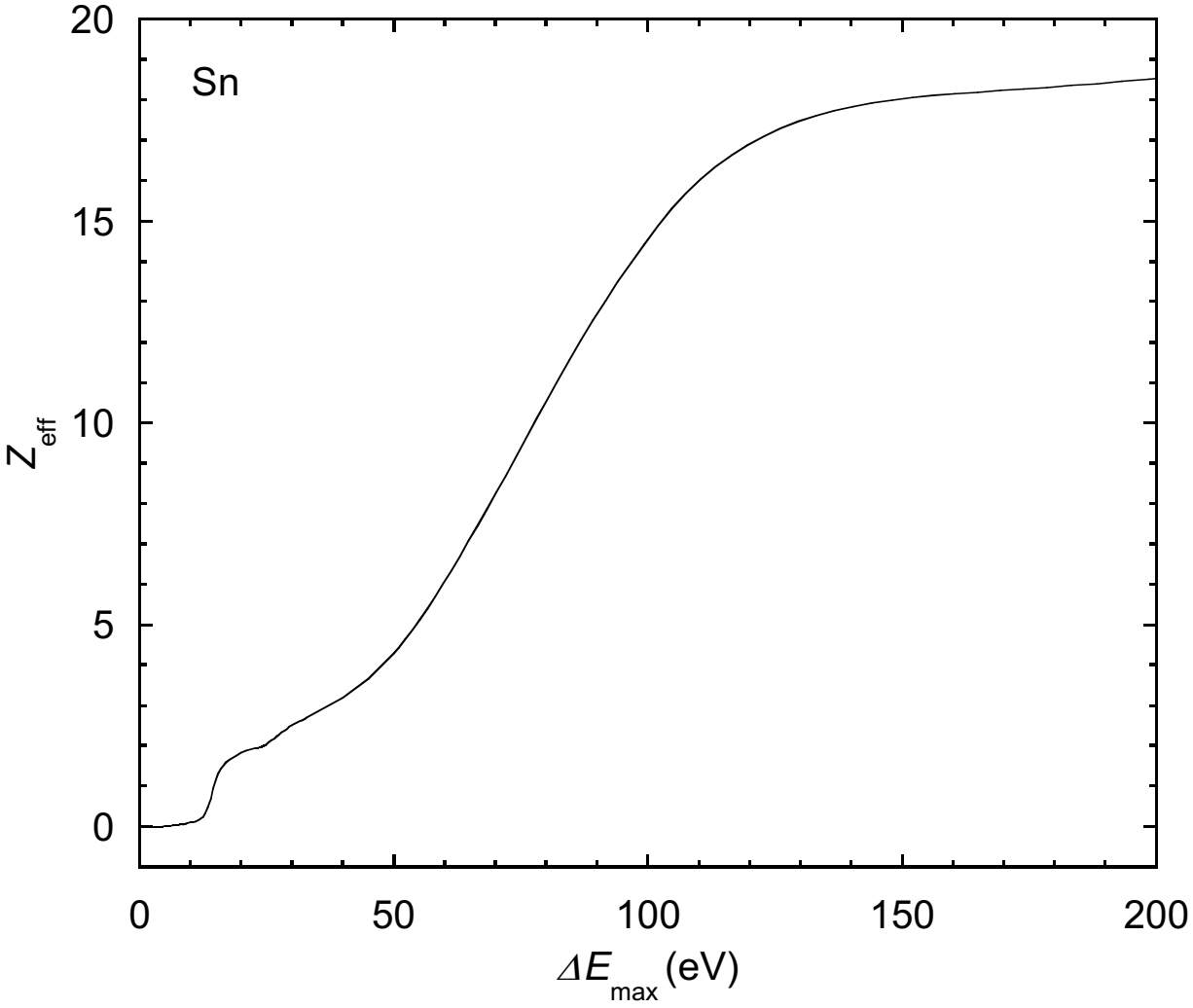

Fig. 21(b).

Author Manuscript:
Published in final edited form as: *Surf. Interface Anal*. Volume 37, Issue 1, Pages 1 - 14 (2005).
https://doi.org/10.1002/sia.1997

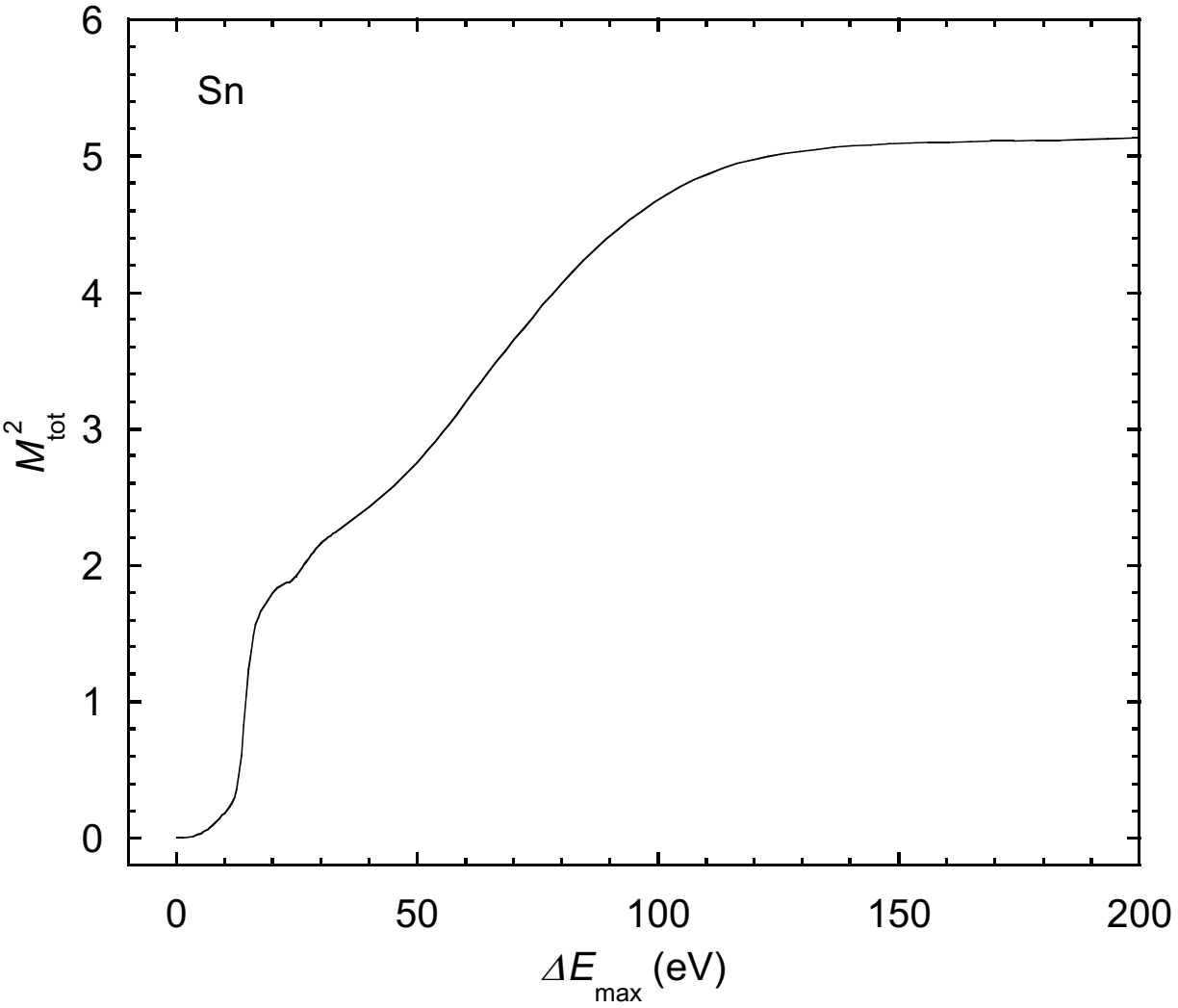

Fig. 21(c).